IEEE Open Journal of the Communications Society

Received XX Month, XXXX; revised XX Month, XXXX; accepted XX Month, XXXX; Date of publication XX Month, XXXX; date of current version 11 January, 2024.

Digital Object Identifier 10.1109/OJCOMS.2024.011100

Time Modulated Arrays Beamforming for Non-Terrestrial Network User Terminal

Gebrehiwet Gebrekrstos Lema[1] ***(Student Member, IEEE)***, **Eva Lagunas** [1] ***(Senior Member, IEEE)***, **Bhavani Shankar M. R.**[1] ***(Senior Member, IEEE)***, **Joel Grotz,**[2] ***(Senior Member, IEEE)***

[1]Interdisciplinary Centre for Security, Reliability and Trust (SnT), University of Luxembourg, Luxembourg
[2]SES, Luxembourg

CORRESPONDING AUTHOR: Gebrehiwet Gebrekrstos Lema (e-mail: gebrehiwet.lema@uni.lu).

This work has been supported by the Luxembourg National Research Fund (FNR) under the project (IPBG19/14016225/INSTRUCT).

ABSTRACT Though beamforming is the fundamental element of satellite communication, it incurs costs, complexity, and power consumption. In this paper, we study a Time-Modulated Array (TMA) beamforming design on the Non-Terrestrial Network (NTN) User Terminal (UT) to receive a signal from a LEO satellite downlink. Despite its simplicity and cost-effectiveness, conventional TMA has intrinsic gain, flexibility, and interference limitations. We compared TMA beamforming with the conventional phased array and studied a tri-state switching method to address the TMA limitations. Based on the 3GPP beam pattern, we studied the beamforming cost and complexity to achieve a viable Signal-To-Noise Plus Interference Ratio (SINR). To facilitate low-cost TMA beamforming, we first derive the Direction of Arrival (DoA) to the TMA switching parameters mapping. Subsequently, we formulate a constrained nonlinear multi-variable problem and solve it using iterative optimization based on perfect DoA. Additionally, we use an analytical approach to suppress sidelobes and unused harmonics using alternating switching. Furthermore, we develop an Alternating Direction Method of Multipliers (ADMM) and Adaptive Switching Parameters Control (ASPC) methods to design TMA beamforming based on a beacon signal. We compare TMA and phased array beamforming techniques, confirming the promising performance of TMA with reduced cost, complexity, and power consumption.

INDEX TERMS NTN UT, TMA, beamforming, satellite communications

I. INTRODUCTION

WHILE Terrestrial Networks (TNs) provide mobile broadband services to the vast majority of developed countries, digital accessibility is limited in rural and sub-urban areas and the least developed countries [1], [2]. Terrestrial infrastructure also becomes unaffordable when considering fast-mobility platforms over the ocean, mountains, or deserts. With connectivity being a key enabler of economic and social development, there has been recently an upsurge in the deployment of NTNs [3]. Recently, Low-Earth Orbit (LEO) constellations of relatively small satellites have started populating our sky in an attempt to provide global connectivity and complement the coverage gap of TNs [4]. The Very Small Aperture Antenna (VSAT) was used in the conventional satellite UT. With satellite mobility gaining momentum and the popularity of LEO constellations, UT needs an urgent adaptation to track satellites on the move. The new UT shall be equipped with smart antennas, ideally with multi-beam capabilities, that can self-align and track the satellite quickly and execute seamless and efficient satellite hand-over.

Omnidirectional UT antennas lack directivity to achieve solid and reliable UT-to-satellite connections. Consequently, manufacturers started investing in terminals with beamforming capabilities using phased arrays [5]. Beamforming enables UTs to communicate with satellites simultaneously and to track and switch between satellites as they move across the sky. Beamforming ensures seamless communica-

This work is licensed under a Creative Commons Attribution 4.0 License. For more information, see https://creativecommons.org/licenses/by/4.0/

tion even as satellites move between coverage areas. Additionally, it allows UTs to focus their transmit and receive signals in specific directions, enhancing the signal quality. On the downside, beamforming (BF) with phased arrays requires complex and expensive hardware requirements and signal processing algorithms, leading to increased costs and complexities. Manufacturing phase shifters with high power handling capabilities and a wide range operating frequency necessitate more sophisticated and adaptable parts, raising overall prices. Hence, phased arrays are costly and pose a barrier for satellite operators to enter the mass market offered by the Fifth-Generation (5G) technology standard for cellular networks. In general, the cost of phase shifters is usually up to nearly half the price of the entire phased array [6]. The enhanced coverage and seamless access to 5G basic services have been the main motivation to introduce NTN solutions into 5G standards [7], [8]. For NTN to succeed in penetrating the 5G market, cost-effective UT antenna solutions are critical. For example, the 5G direct access for vehicles (5G-V2X) is one of the use cases where NTN can have a substantial impact, as NTN can offer ubiquitous coverage for connected vehicles [9]. While the satellite-to-ground beams are broad and can match wide-spread mobility patterns, the UT antennas shall offer enough gain towards the sky while occupying a limited surface and with a low production cost.

This paper investigates TMA for NTN-UTs. The main motivation for this technology is the practical implementation of TMA, which considers the use of switches rather than complex weight multiplications. In the next section, we provide an overview of the relevant state of the art and highlight the main contributions of our work.

A. STATE OF THE ART

The typical antenna of NTN-UT is a parabolic antenna, commonly known as *dish* antenna. The *dish* antenna became very popular with geostationary satellites. The advent of LEO constellations posed significant challenges to the NTN-UT antenna. European Space Agency (ESA) research team has demonstrated a re-configurable Ka-band NTN-UT antenna based on a low-profile active phased-array, [10]. Similarly, CesiumAstro, SES, and Hughes have successfully demonstrated scalable phased array NTN-UTs with a seamless connection with satellites and mobile platforms, [11]. The challenge of electronically steerable antennas resides in their implementation cost/complexity, power consumption, and the design of appropriate beamforming coefficients for the beam steering at a fast pace to track the moving satellite.

The literature widely considered analog and digital beamforming. In Analogue Beamforming (ABF), the amplitude and phase variation are applied to the analog signal at each element and then combined before the Analog-to-Digital Conversion (ADC), [12]. However, an N element with L-stream fully ABF receiver requires L RF-front ends and a linear BF network with $L \times N$ phase shifters, [13]. This is still simpler than the Digital Beamforming (DBF). DBF performs the amplitude and phase variation in the digital domain, thus requiring a dedicated Radio-Frequency (RF) chain with individual Digital-to-Analog Converter (DAC) for each antenna element, [14]. The complexity of BF increases with the number of elements in addition to the size and weight cost. A few array elements can be designed to generate multiple beams using Butler-matrix [15]. However, it is costly and complex to implement in the NTN-UT. An N element Butler matrix generates N beams using $N \times N$ matrix networks, N phase shifters, $2N$ crossovers, and more than N quadrature hybrid, [16], [17].

TMAs replace the expensive phase shifters of phased arrays with on-off switching to control the radiation patterns. The switching pulses generate Sidebands (SBs), which were treated as a drawback for decades, and researchers were suppressing the SBs [18], [19]. Recently, a few research have been conducted to exploit the multiple sideband properties for harmonic beamforming [20], and others applied the TMA for direction finding, [21]. Despite their processing and BF network simplicity [22], TMAs have intrinsic gain, flexibility, and interference limitations. TMAs exhibit a noticeable energy leakage due to the off times, resulting in significant SINR degradation. Complex structure [23], variable-gain amplifiers, and analog multipliers [24] were studied to circumvent the drawback. However, these methods sacrifice beamforming flexibility and complexity. The radiation pattern control using TMA switching has been studied, [25], [26]. Similarly, [27] studied the switching sequences and optimum element positions to reduce the SLLs and suppress the SBs in 5G wideband applications. Multiple Input Multiple Output (MIMO) systems have gained significant spectral efficiency and data rates; however, the multiple RF chains result in high hardware complexity, array size, and cost. For this reason, driven by its single RF chain, TMA has been studied as a replacement for MIMO systems, [28]. The demand for TMA is widely attracting industries in the TNs and NTNs. Inspired by its additional control parameter and directional beams, on its recent call for secure satellite communication, the ESA highlights the significance of TMA works, such as [29], [30], for the success of the project. The applicability of TMA-based BF was studied for satellite communication applications, [31]. The direction finding and multi-beam characteristics made TMA a promising potential for satellite applications. The theoretical pattern synthesis of TMA structure was studied for GEO and MEO satellite applications [32]. However, neither the satellite system beam steering nor advanced signal processing methods have been studied to improve the TMA beamforming capabilities. This work builds upon previous authors' work [33], where TMA was applied onboard the satellite. In this work, we study TMA beamforming on the UT using advanced methods, including QPO, ADMM, and ASPC. Additionally, we compare the cost, complexity, and power consumption of the

This article has been accepted for publication in IEEE Open Journal of the Communications Society. This is the author's version which has not been fully edited and content may change prior to final publication. Citation information: DOI 10.1109/OJCOMS.2024.3522519

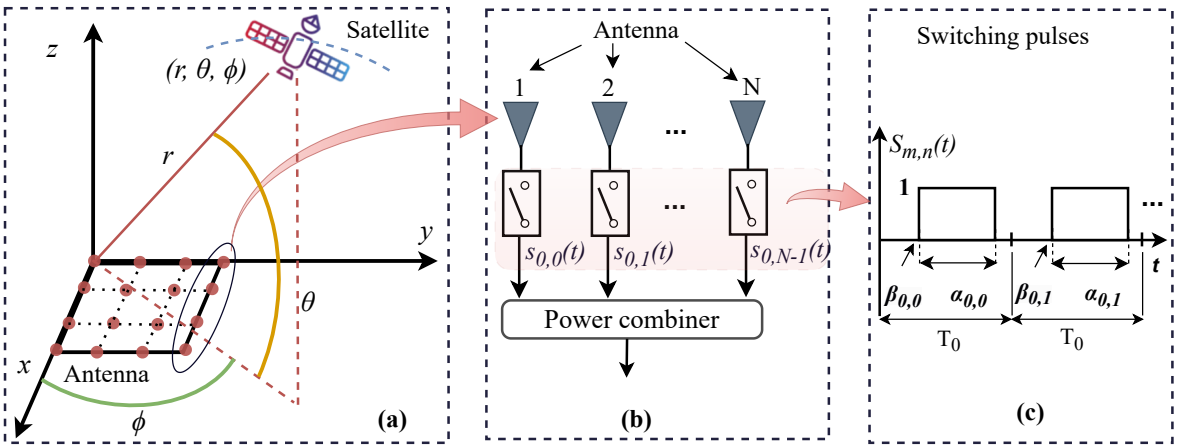

Figure 1: (a) Geometry of satellite to UT antenna array link, (b) the first column of the UT antenna array magnified (forming simplified TMA structure), and (c) on-off switching pulses

proposed TMA beamforming with the conventional phased array beamforming.

B. CONTRIBUTIONS

To the best of the authors' knowledge, this is the first work that studies TMA beamforming for NTN-UT. In particular, this work leverages the simplicity of TMA beamforming for UT communicating with LEO satellite systems. The novelty of the paper with respect to [33] includes the introduction of advanced signal processing schemes on TMA beamforming for NTN UT communications. The rest of the novelty and contributions of this paper are summarized as follows:

- We study the performance, cost, and complexity trade-offs of the conventional phased array and TMA.
- We formulate DoA to TMA parameters mapping, the SINR maximization problem, and we have discussed the cost and complexity required to attain viable SINR.
- To show the practicality of TMA, we evaluate the channel estimation imperfection errors due to LEO satellite mobility under different beam shapes.
- To fill the gain and flexibility limitation of conventional TMA, we studied alternating switching. Additionally, we formulate an analytical method to remove unused sidebands, suppress SLL, and beamform in the DoA while maintaining low implementation costs.
- We formulate the TMA beamforming as a multi-objective problem to optimize SLL and directivity as a function of TMA switching parameters in a given DoA. We solved the problem using a standard tool and compared the performance with previous works.
- A novel signal processing techniques are introduced to design TMA beamforming based on a beacon signal.
- We compare the cost and complexity of the conventional phased array and TMA beamforming, confirming the superiority of TMA.
- We demonstrate that TMA beamforming offers considerable power consumption benefits compared to conventional analog and digital beamforming methods.

The rest of the paper is structured as follows: Section II discusses the TMA fundamentals, including the TMA radiation pattern and downlink signal models. Section III covers TMA beamforming approaches. Section IV formulates TMA beamforming for NTN communications. Section V simulates and discusses the numerical results. Finally, Section VI summarises the paper.

II. TMA FUNDAMENTALS

We consider the downlink scenario where a LEO satellite establishes communication with a UT equipped with TMA. The LEO satellite transmits the signal to the UT following the 3GPP recommendations for NTN systems [7]. This NTN UT shall steer the beam towards the LEO satellite to maximize the quality of the received signal.

A. TMA RADIATION PATTERN

The elements of a Uniform Planar Array (UPA) are given in the xy plane with a total of $M \times N$ elements, making it 2D TMA by integrating switches instead of phase shifters, as shown in Fig. 1(a). The position of the satellite is given by (r, θ, ϕ), where θ and ϕ are the elevation and azimuth angles of the satellite, respectively, $w.r.t$ the NTN UT. The 2D TMA Array Factor (AF) is given as

$$AF(\theta, \phi, t) = \sum_{n=0}^{N-1} \sum_{m=0}^{M-1} I_{m,n} S_{m,n}(t) \\ e^{jk(nd_y \sin\theta \cos\phi + md_x \sin\theta \sin\phi)}, \quad (1)$$

where d_x and d_y are the element spacing in the x-direction and y-direction, respectively. $S_{m,n}(t)$ is a switching function of the $(m,n)^{th}$ element of the array, $k = 2\pi/\lambda$ is the wavenumber related to the carrier frequency f_c, $F_0 = 1/T_0$ is the modulating frequency, and T_0 is the period. $I_{m,n} =$

$|A_{m,n}|e^{-j\phi_{m,n}}$ is the polar form of the complex static excitation of the $(m,n)^{th}$ element and we assume $I_{m,n}=1$ unless specified, $n=0,1,...,N-1$, and $m=0,1,...,M-1$. The first column of the UPA elements is shown in Fig. 1 (b), and RF switches are integrated into every element. The normalized switching pulse width and delay of the $(m,n)^{th}$ element are $\alpha_{m,n}$ and $\beta_{m,n}$, respectively, as shown in Fig. 1 (c). By adopting the Fourier series-based approach from our recent paper [33], the complete 2D TMA AF is given by:

$$AF(\theta,\phi,t)=\sum_{q=-Q}^{Q}e^{j(\omega_c+q\omega_0)t}\sum_{n=0}^{N-1}\sum_{m=0}^{M-1}\alpha_{m,n}\,\mathrm{sinc}(\pi q\alpha_{m,n})\\ e^{-j\pi q(\alpha_{m,n}+2\beta_{m,n})}e^{jk(nd_y\sin\theta\cos\phi+md_x\sin\theta\sin\phi)}, \tag{2}$$

where, $\omega_c=2\pi f_c, \omega_0=2\pi F_0$, and q is the TMA sidebands.

A simplified switching function for the first column of the 2D TMA is represented by the $(0,n)^{th}$ switch as shown in Fig. 1 (b) and (c). The first column is, henceforth, represented by the n^{th} term for brevity. To model the TMA radiation pattern, for the sake of simplicity and without loss of generality, we present the subsequent notation with 1D, where the n^{th} element is controlled by the n^{th} RF-switch $S_n(t)$ as:

$$S_n(t)=\begin{cases}1, & \text{if } \tilde{\beta}_n\le t\le\tilde{\alpha}_n\\ 0, & \text{otherwise.}\end{cases} \tag{3}$$

where, $\tilde{\alpha}_n$ and $\tilde{\beta}_n$ denote the OFF and ON switching instants of $S_n(t)$, respectively. The normalized duration α_n and delay β_n of the n^{th} element are related to the instant switching as $\alpha_n=(\tilde{\alpha}_n-\tilde{\beta}_n)/T_0$ and $\beta_n=\tilde{\beta}_n/T_0$. The AF of the simplified 1D TMA in θ direction $w.r.t$ the $z-$axis is:

$$AF\,(\theta,t)=\sum_{n=0}^{N-1}e^{j2\pi f_c t}S_n(t)I_n e^{jnkd\cos(\theta)}, \tag{4}$$

where d is the inter-element spacing. The Fourier coefficients $\tilde{S}_{n,q}$ due to the RF-switching $S_n(t)$ is given as:

$$S_n(t)=\sum_{q=-\infty}^{\infty}\tilde{S}_{n,q}e^{jq2\pi F_0 t}, \tag{5}$$

Then, by substituting equation (5) in (4), the AF is:

$$AF(\theta,t)=\sum_{q=-\infty}^{\infty}\sum_{n=0}^{N-1}\tilde{S}_{n,q}I_n e^{jnkd\cos(\theta)}e^{j2\pi(f_c+qF_0)t}. \tag{6}$$

Using Fourier theory, $\tilde{S}_{n,q}$ is computed as [18]:

$$\tilde{S}_{n,q}=\alpha_n\,\mathrm{sinc}(\pi q\alpha_n)e^{-j\pi q(2\beta_n+\alpha_n)}. \tag{7}$$

Finally, by substituting (7) into (6), the 1D TMA AF is:

$$AF(\theta,t)=\sum_{q=-Q}^{Q}\sum_{n=0}^{N-1}I_n\alpha_n\,\mathrm{sinc}(\pi q\alpha_n)e^{-j\pi q(\alpha_n+2\beta_n)}\\ e^{jnkd\cos(\theta)}e^{j2\pi(f_c+qF_0)t}. \tag{8}$$

From (8), it is evident that the TMA switching parameters, α_n and β_n determine the beam shape and direction of the beam, a motivation to replace the phased array with TMA. We can also shape the beamwidth without significantly increasing the array size.

B. DOWNLINK RECEIVER SIGNAL MODEL

The block diagram shown in Fig. 2 indicates the system employing a TMA receiving beamforming structure. Let $b(t)$ be the baseband signal at the satellite with $\mathbb{E}[|b(t)|^2]=1$. We assume signals are impinging from different directions depending on the location of the LEO satellite. The signal transmitted by the satellite is defined by $\tilde{c}(t)$ as,

$$\tilde{c}(t)=\sqrt{p}b(t)e^{j2\pi f_c t}, \tag{9}$$

where p is the satellite transmit power per beam. The channel from the satellite to the n^{th} element of the UT can be represented as h_n. We have $h_n=D_n e^{-j2\pi f_D t}$, where, D_n is the complex channel gain at the n^{th} element and f_D is the Doppler shift. For every DoA θ, the Doppler shift is given by $v_r\cos(\theta)f_c/c$. where v_r is the relative velocity of the satellite $w.r.t$ the UT and c is the speed of light. Assuming a noiseless narrowband signal received by the first element $c(t)$, the signal received at the n^{th} element is:

$$r_n(t)=x_n(t)e^{j2\pi f_c t}a_n(\theta)+\eta_n(t), \tag{10}$$

where $x_n(t)=h_n c(t)$, $a_n(\theta)=e^{jnkd\cos(\theta)}$, and $\eta_n(t)$ is assumed to be white Gaussian noise. The received signal undergoes the time modulation using $S_n(t)$ as:

$$y_n(t)=S_n(t)r_n(t). \tag{11}$$

The modulated signal $y_n(t)$ is combined to yield $y(t)$ as:

$$y(t)=\sum_{n=0}^{N-1}S_n(t)r_n(t), \tag{12}$$

Subsequently, by including the Fourier series coefficient, $\tilde{S}_{n,q}$, the received signal can be represented as:

$$y(t)=\sum_{q=-\infty}^{\infty}\left[\sum_{n=0}^{N-1}\tilde{S}_{n,q}r_n(t)e^{j2\pi qF_0 t}\right]. \tag{13}$$

The expression in (13) comprises harmonic components of the form f_c+qF_0. Retaining a finite number of them yields:

$$y(t)\approx\sum_{q=-Q}^{Q}e^{j2\pi qF_0 t}\left[\sum_{n=0}^{N-1}\tilde{S}_{n,q}x_n(t)a_n(\theta)\right]. \tag{14}$$

Finally, as shown in Fig. 2, the analog signals are converted to baseband with the harmonic components distinguished by using Band Pass Filters (BPFs) centred around qF_0 as

$$y_q[l]=\sum_{n=0}^{N-1}\tilde{S}_{n,q}x_n(lT_0)a_n(\theta)+\eta_q[lT_0], \tag{15}$$

where l is an integer, lT_0 is the discrete-time samples, $\eta_q(t)$ is the noise after Fourier decomposition, and $T_s=lT_0$. To avoid signal distortion, the symbol period T_s is assumed to be at least 5 times larger than the modulation period T_0, which increases the granularity of time modulation within the symbol period. Generally, the TMA switching time is

This article has been accepted for publication in IEEE Open Journal of the Communications Society. This is the author's version which has not been fully edited and content may change prior to final publication. Citation information: DOI 10.1109/OJCOMS.2024.3522519

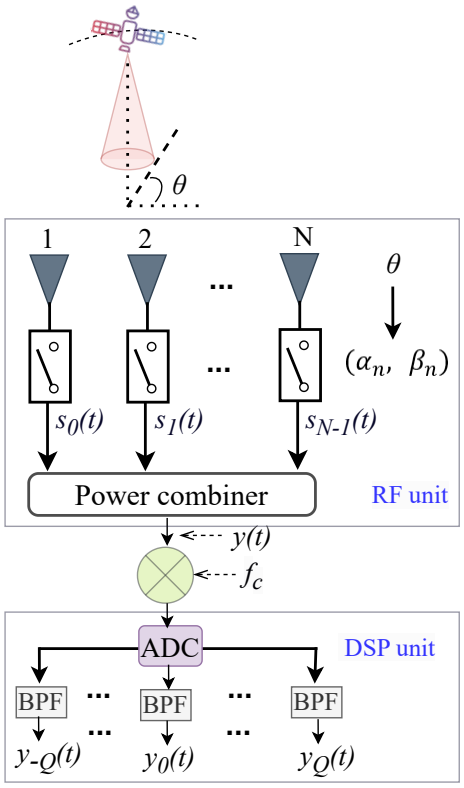

Figure 2: TMA beamforming at the NTN UT: compute switching parameters based on DoA and time modulation using the switching parameters (RF unit) and filter target frequency at the Digital Signal Processing (DSP) unit

faster than the modulation period. Hence, faster switches are preferred because a shorter modulation duration makes a greater data rate possible. The terms θ, α_n and β_n shown in Fig. 2 indicate the DoA of the satellite signal to TMA switching parameters mapping.

III. TMA BEAMFORMING APPROACHES

In this section, we first formulate the alternating switching technique and its significance in TMA beamforming. Then, we formulate the mathematical relationship of the DoA and the TMA switching parameters. Finally, we study the SLL and noise suppression, as well as the cost and complexity of the TMA to enhance the SINR.

A. TMA WITH ALTERNATING SWITCHING TECHNIQUE

So far, the switching type was single-pulse on-off RF-switches, as shown in Fig. 1 (c). Despite its simplicity, conventional single-pulse switching has limitations such as low gain, many harmonics, and a lack of beamforming with the fundamental component. From (8), the fundamental component ($q = 0$) is phase-independent, and the beamforming is impossible with it. So, it does not apply to LEO satellite systems and consumes much power without being used for beamforming. It can also introduce interference on other links working at the same frequency. Hence, to overcome these limitations, we studied a tri-state switching with an additional degree of freedom as shown in Fig. 3, and mathematically represented as:

$$g_n(t) = \begin{cases} 1, \ \tilde{\beta}_n^{(1)} < t \leq \tilde{\alpha}_n^{(1)} \\ -1, \ \tilde{\beta}_n^{(2)} < t \leq \tilde{\alpha}_n^{(2)} \\ 0, \text{ otherwise in } [0, T_0]. \end{cases} \tag{16}$$

Recall that T_0 is the modulation period, $(\tilde{\beta}_n^{(1)}, \tilde{\alpha}_n^{(1)})$ and $(\tilde{\beta}_n^{(2)}, \tilde{\alpha}_n^{(2)})$ are the switching ON and OFF instants for the positive and negative cycles, respectively. Since $g_n(t)$ are periodic functions, their Fourier series expansion is:

$$g_n(t) = \sum_{q=-\infty}^{\infty} G_{n,q} \mathrm{e}^{\mathrm{j}2\pi q F_0 t}. \tag{17}$$

$G_{n,q}$ is the q^{th} Fourier coefficient of the n^{th} switching function and they can be calculated as,

$$\begin{aligned} G_{n,q} &= \frac{1}{T_0} \int_0^{T_0} g_n(t) e^{-j2\pi q F_0 t} \, \mathrm{d}t, \\ &= \alpha_n^{(1)} \operatorname{sinc}(\alpha_n^{(1)} q) e^{-jq\pi\left(2\beta_n^{(1)} + \alpha_n^{(1)}\right)} \\ &\quad - \alpha_n^{(2)} \operatorname{sinc}(\alpha_n^{(2)} q) e^{-jq\pi\left(2\beta_n^{(2)} + \alpha_n^{(2)}\right)}, \end{aligned} \tag{18}$$

where, $\alpha_n^{(i)} = (\tilde{\alpha}_n^{(i)} - \tilde{\beta}_n^{(i)})/T_0$ and $\beta_n^{(i)} = \tilde{\beta}_n^{(i)}/T_0$ are the normalized durations and delays, respectively, for $i = 1$ or 2. From (18), the beam steering is again impossible at $q = 0$. However, using $\alpha_n^{(1)} = \alpha_n^{(2)} = \alpha_n$, we can remove the $q = 0$ component and the power distributes to the useful SBs, and (18) reduces to:

$$\begin{aligned} G_{n,q} &= \alpha_n \operatorname{sinc}(\alpha_n q) e^{-jq\pi\alpha_n} [e^{-j2q\pi\beta_n^{(1)}} - e^{-j2q\pi\beta_n^{(2)}}] \\ &= B_{n,q} e^{j\varphi_{n,q}} \end{aligned} \tag{19}$$

Using the Euler and trigonometric methods, we provided the details in Appendix 1 that (19) can be represented as:

$$\begin{aligned} B_{n,q} &= \frac{2}{\pi q} \sin(q\pi\alpha_n) \sin q\pi \left(\beta_n^{(2)} - \beta_n^{(1)}\right), \\ \varphi_{n,q} &= -q\pi \left(\alpha_n + \beta_n^{(1)} + \beta_n^{(2)}\right) + \frac{\pi}{2}. \end{aligned} \tag{20}$$

From Fig. 3, we can observe that $\alpha_n^{(1)} + \alpha_n^{(2)} \leq 1$ and then, for the $\alpha_n^{(1)} = \alpha_n^{(2)} = \alpha_n$ case, we can deduce that, $\alpha_n \leq 1/2$. Furthermore, to maximize $B_{n,q}$, we must set $\beta_n^{(2)} - \beta_n^{(1)} = 1/2$ for the first harmonic component $B_{n,1}$. The reason we choose the first harmonic component is because the highest gain attains at $B_{n,1}$, as can be shown from (20). Therefore, we steer the beam of the first harmonics using $\beta_n^{(1)}$, and we can calculate $\beta_n^{(2)}$ directly from the relationship of $\beta_n^{(2)} = \beta_n^{(1)} + 1/2$.

The 1D TMA AF employing alternating switching is:

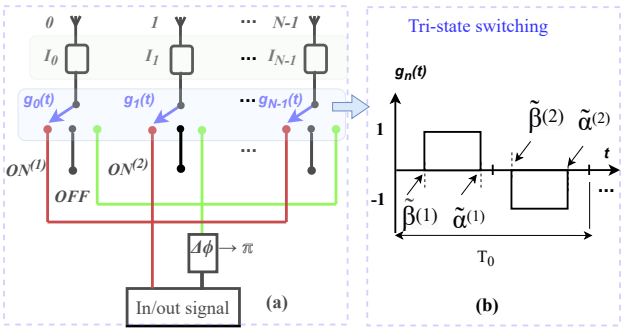

Figure 3: Alternating switching (a) structure and (b) pulses

$$AF(\theta,t)=\sum_{q=-Q}^{Q}\sum_{n=0}^{N-1} I_n G_{n,q} e^{jnkd\cos(\theta)} e^{j2\pi(f_c+qF_0)t} \tag{21}$$

The 2D TMA with the alternating switching for $q=1$ is:

$$\begin{aligned} AF(\theta,\phi,t) &= \sum_{n=0}^{N-1}\sum_{m=0}^{M-1} I_{m,n} g_{m,n}(t) \\ &\quad e^{jk(nd_y\sin\theta\cos\phi+md_x\sin\theta\sin\phi)} e^{j2\pi f_c t}, \\ &= \sum_{n=0}^{N-1}\sum_{m=0}^{M-1} I_{m,n} G_{m,n,1} \\ &\quad e^{jk(md_x\sin\theta\cos\phi+nd_y\sin\theta\sin\phi)} e^{j2\pi(f_c-F_0)t}, \end{aligned} \tag{22}$$

where $G_{m,n,1} = \alpha_{m,n}\,\mathrm{sinc}(\alpha_{m,n}) e^{-j\pi\alpha_{m,n}}[e^{-j2\pi\beta^{(1)}_{m,n}} - e^{-j2\pi\beta^{(2)}_{m,n}}]$. Here $g_{m,n}(t)$ is the 2D alternating switching function, and the Fourier coefficients of the first harmonic are $G_{m,n,1} = B_{m,n,1} e^{j\varphi_{m,n,1}}$, where

$$\begin{aligned} B_{m,n,1} &= \frac{2}{\pi}\sin(\pi\alpha_{m,n})\sin\pi\left(\beta^{(2)}_{m,n}-\beta^{(1)}_{m,n}\right), \\ \varphi_{m,n,1} &= -\pi\left(\alpha_{m,n}+\beta^{(1)}_{m,n}+\beta^{(2)}_{m,n}\right)+\frac{\pi}{2}. \end{aligned} \tag{23}$$

B. TMA BEAM STEERING

In this subsection, for successful beamforming on the NTN UT, we show the satellite DoA to the TMA switching parameter mapping. To formulate the DoA to the TMA switching parameter mapping, we cover both the conventional TMA (single-pulse switching) and the alternating switching TMA in their 1D and 2D structures.

1) DoA to single-pulse switching parameters mapping in 1D

The satellite signal DoA to the TMA switching parameters (α_n, β_n) mapping has two-fold objectives: (1) map the satellite position to the TMA switching parameters to steer the main lobe and (2) assess the impact of TMA sidelobes through SINR. We use lower $|q|$ so that sinc(.) is closer to 1, impacting the signal strength as shown in (24b). To formulate the TMA beam steering, we rewrite (13) as:

$$\begin{aligned} AF(\theta,t) &= \sum_{q=-Q}^{Q}\sum_{n=0}^{N-1} C_n^q e^{j[nkd\cos\theta-\pi q(\alpha_n+2\beta_n)]} \\ &\quad e^{j2\pi(f_c+qF_0)t}, \end{aligned} \tag{24a}$$

$$C_n^q = \alpha_n\,\mathrm{sinc}(\pi q\alpha_n) = \frac{\sin(\pi q\alpha_n)}{\pi q},\ \text{let } I_n=1, \tag{24b}$$

where we have used $\mathrm{sinc}(x) = \sin(x)/x$, and assume C_n^q being Chebyshev distribution. From the $AF(\theta,t)$ shown in (24a), the phase part is used for the beam steering. For a small value of ϑ, the trigonometric function $\mathrm{sinc}(\vartheta)$ tends to unity. The beam steering at the desired angle θ, is calculated by equating the phase term of (24a) to 0:

$$[nkd\cos\theta - \pi q(\alpha_n+2\beta_n)] = 0. \tag{25}$$

Solving for β_n, with $d=\lambda/2$ and remembering $k=2\pi/\lambda$, the relationship between θ, α_n, and β_n is given as:

$$\beta_n = \frac{1}{2}[n\cos\theta-\alpha_n] = \frac{1}{2}[n\cos\theta - \sin^{-1}(\pi|C_n^1|)]. \tag{26}$$

Hence, TMA beams can be directed using the TMA switching parameters. For the normalized case, the excitation weight has to vary within $[0,1]$. Therefore, $\sin(\pi\alpha_n)$ has to vary within $[0,1]$. Hence, α_n varies in the range $[0,0.5]$.

2) DoA to single-pulse switching parameters mapping in 2D

To direct the beam to the DoA (θ',ϕ'), the time delay $\beta_{n,m}$ is equivalent to the progressive phase shift in the narrow band frequency domain. Hence from (2), by setting the phase term to 0, we formulate the 2D beam steering as:

$$\beta_{m,n} = \frac{k}{2\pi}[nd_y\sin\theta'\cos\phi' + md_x\sin\theta'\sin\phi'] - \frac{\alpha_{m,n}}{2} \tag{27}$$

3) DoA to alternating switching parameters mapping in 1D

For the first harmonic component, $\beta_n^{(2)} - \beta_n^{(1)} = 1/2$ maximizes the AF given in (20). So, determining $\beta_n^{(2)}$ or $\beta_n^{(1)}$ is sufficient to define the beam steering. Using the phase term of (20) and (21), we formulate the beam steering as $jnkd\cos\theta - \varphi_{n,1} = 0$. Then, by solving for $\beta_n^{(1)}$, we derive the beam steering of the first harmonic component as:

$$\beta_n^{(1)} = \frac{1}{2}[\frac{nkd\cos\theta}{\pi} - \alpha_n],\ \beta_n^{(2)} = \beta_n^{(1)} + 1/2. \tag{28}$$

4) DoA to alternating switching parameters mapping in 2D

For the satellite position (θ',ϕ'), using the phase of the AF given in (22), we derive the 2D beam steering using $jk\,(nd_y\sin\theta\cos\phi + md_x\sin\theta\sin\phi) - \varphi_{m,n,1} = 0$. Solving for $\beta^{(1)}_{m,n}$, we formulate the 2D beam steering as:

$$\begin{aligned} \beta^{(1)}_{m,n} &= \frac{k}{2\pi}[nd_y\sin\theta'\cos\phi' + md_x\sin\theta'\sin\phi'] - \frac{\alpha_{m,n}}{2}, \\ \beta^{(2)}_{m,n} &= \beta^{(1)}_{m,n} + 1/2. \end{aligned} \tag{29}$$

C. SLL AND NOISE SUPPRESION

This subsection studies the SLL and noise suppression with the TMA structure to maximize SINR. We cover the SLL and the beam shape impacts on SINR and the cost and complexity needed to attain a viable SINR.

The main objective is to optimize the TMA switching parameters such that the TMA beam accurately points to the moving LEO satellite to have optimal SINR. The additional objective is to study the impact of SLL and the beam shape of TMA on SINR. To formulate the problem, we consider the equation that links the DoA angle with the TMA switching parameters formulated in section B (B). Subsequently, we formulate the SINR maximization problem as a function of the switching parameters. While the principle is the same, for simplicity in the subsequent sections, we use single-pulse switching unless specified.

Considering multibeam LEO satellite configuration with full frequency reuse similar to [34] and [35], we evaluate the SINR maximization using TMA parameters. The signal power of the satellite received by the first harmonic component of the target UT is represented as $|h_n AF(\theta,t)|^2 p$, where $AF(\theta,t)$ is the antenna response at the first harmonic component with DoA θ. Here, p is the transmit power over the channel h_n. An inter-beam interference can occur on the target UT when other beams $\tilde{q}$ work with the same carrier. The interfering power coming from the other beams serving using the $\tilde{q}^{th}$ harmonic component over the channels $h_{n,\tilde{q}}$ can be defined as $\sum_{\tilde{q}=-Q}^{Q} |h_{n,\tilde{q}} AF_{\tilde{q}}(\theta,t)|^2 p_{\tilde{q}}$, where $|AF_{\tilde{q}}(\theta,t)|^2$ is $\tilde{q}^{th}$ interfering source with the power per the $\tilde{q}^{th}$ beam of $p_{\tilde{q}}$. The SINR at the target UT is the ratio of the power received by the noise plus the interference from other beams, summarized as:

$$SINR = \frac{|h_n AF(\theta,t)|^2 p}{\varsigma \sigma_{\tilde{q}}^2 + \sum_{\tilde{q}=-Q,\tilde{q}\neq q}^{Q} |h_{n,\tilde{q}} AF_{\tilde{q}}(\theta,t)|^2 p_{\tilde{q}}},$$
$$\text{here, } |AF_{q_K}(\theta,t)|^2 = \sum_{n=0}^{N-1} |\tilde{S}_{n,q_K} e^{jnkd\cos(\theta)}|^2, \tilde{q} \neq q, \tag{30}$$

where $q_K = 1$ for the desired signal and $q_k = \tilde{q}$ for the interfering signal, ς is the noise bandwidth, and $\sigma_{\tilde{q}}^2$ is the $\tilde{q}^{th}$ AWGN. From (30), the SINR largely depends on (i) the Sidelobe Level (SLL) or gain of the TMA, (ii) the beamwidth, and (iii) the separation between the beams. In this paper, we use the TMA switching parameters to maximize the SINR, and we formulate it for $q = 1$ as:

$$\begin{aligned} & \max_{\alpha_n} SINR, \\ Where: \quad & C_n^1 = \frac{\sin(\pi\alpha_n)}{\pi}, \forall n \\ & \beta_n = \frac{1}{2}[\frac{nkd\cos\theta}{\pi} - \alpha_n], \\ s.t. \quad & 0 \leq \alpha_n \leq \ 0.5. \end{aligned} \tag{31}$$

From (31), C_n^1 as given in (24b) and β_n define the antenna response's overall excitation amplitude and phase control, respectively. The constraint represents the normalized switching duration of the TMA. We studied the SINR performance effects of gain/SLL, beamwidth, and Chebyshev windowing. We compared the SINR performance of alternating switching with the conventional TMA and phased array while considering the implementation cost and complexity.

The impact of SLL and gain on SINR is interchangeable, as reducing SLL increases gain in the same aperture and array structure. First, we formulate the peak value of the main lobe as $AF_\theta = \max_\theta |AF(\theta,t)|^2$ and then we determine the maximum SLL and the relative SLL (in dB), respectively:

$$AF_{\tilde{\theta}} = \max_{\tilde{\theta},\tilde{\theta}\neq\theta} |AF(\theta,t)|^2, \text{SLL} = 20\log_{10}(AF_{\tilde{\theta}}/AF_\theta), \tag{32}$$

where AF_θ and $AF_{\tilde{\theta}}$ are the maximum of the AF in the main lobe and the SLL, respectively. Further details on beamwidth, SLL, and alternating switching are given in Section IV.

Similarly, the Chebyshev technique applied to the excitation weight C_n^1 of (31) is used to maximize the SINR by playing with the SLL, beamwidth, and cost-complexity tradeoffs. We consider the Chebyshev Tapering detailed in [36].

IV. TMA-BASED RECEIVER BEAMFORMING FOR NTN COMMUNICATIONS

Section III covers signal quality-improving strategies by relying on beam steering, beam spacing, SLL, or gain. In this section, we extend the beamforming solutions to enhance beam shape, adaptability to rapid changes, and robustness to mobility effects, simplifying NTN communication implementation. We present the proposed solutions in two major categories: perfect and imperfect DoA. In the first category, we have introduced a novel analytical approach to suppress SLLs and unused harmonics. Next, we convert the problem into a constrained nonlinear multivariable function, which can be solved with iterative optimization. This includes optimizing the switching parameters using quadratic programming to enhance SLL and directivity. The second category focuses on designing the TMA switching parameters and estimating the DoA θ by relying on a beacon signal, which performs without frequent channel state DoA information, simplifying implementation. The second category is subdivided into ADMM and ASPC methods.

A. DYNAMIC BEAMFORMING USING PERFECT DoA

In this section, we first formulate a general BF problem for a perfect DoA and analytically show the potential alternating switching. Second, we reformulate the problem and outline an optimization algorithm. With the conventional on-off switching TMA, the fundamental component and

other harmonics continue to be a source of interference and power leakage. Therefore, we need to reduce the number of sidebands (SBs) in general and non-beamforming SBs in particular. Hence, the objectives of this analytical method are (i) to remove the harmonics that cannot be applied for beamforming applications, (ii) to suppress SLL in the beamforming SB, and (iii) to beamform in the desired direction by employing alternating switching.

The AF in (21) is synthesized from the alternating switching, and it can be expressed as $\mathbf{G}_q\mathbf{A}_\theta$, where $\mathbf{G}_q$ and $\mathbf{A}_\theta$ are the Fourier coefficients and the vector guide, respectively:

$$\begin{aligned}\mathbf{G}_q &= [a_{0,q}, a_{1,q}, \cdots, a_{N-1,q}],\\ \mathbf{A}_\theta &= diag[1, e^{jkd\cos(\theta)}, \cdots, e^{j(N-1)kd\cos(\theta)}]^T,\end{aligned}$$

where $a_{n,q} = \alpha_n \operatorname{sinc}(\alpha_n q)e^{-jq\pi\alpha_n}[e^{-j2q\pi\beta_n^{(1)}} - e^{-j2q\pi\beta_n^{(2)}}]$ Then, the general optimization problem is formulated as,

$$\begin{aligned}&\min |\mathbf{A}_{\tilde{\theta}}\mathbf{G}_q|, \tilde{\theta} \in \Omega_0,\\ &\min -|\mathbf{A}_{\theta_q}\mathbf{G}_q|, \theta_q \in \Omega_q,\\ &\min |\mathbf{A}_{\theta_{\tilde{q}}}\mathbf{G}_{\tilde{q}}|, \theta_{\tilde{q}} \in \Omega_{\tilde{q}}, q \neq \tilde{q}\\ \text{s.t. } &|\mathbf{A}_{\theta_0}\mathbf{G}_q| = 1\end{aligned} \tag{33}$$

where, $|\mathbf{A}_{\tilde{\theta}}\mathbf{G}_q|$, $|\mathbf{A}_{\theta_q}\mathbf{G}_q|$, and $|\mathbf{A}_{\theta_{\tilde{q}}}\mathbf{G}_{\tilde{q}}|$ are the antenna response in the SLL direction, in the q^{th} beamforming SB direction, and in the the $\tilde{q}^{th}$ undesired SB direction, respectively.

The domains, $\{\Omega_0, \Omega_q, \Omega_{\tilde{q}}\}$ refer to the SLL region of the beamforming SBs, beamforming SB, and non-beamforming SBs, respectively. $|\mathbf{A}_{\theta_0}\mathbf{G}_q| = 1$ indicates the maximum normalized gain of the q^{th} beamforming sideband of the main lobe.

This work proposes a simple but efficient analytical approach to solve the problem given in (33). From the alternating switching given in (19), $B_{n,q}$ reduces to $\frac{2}{\pi q}\sin(q\pi\alpha_n)\sin q\pi(\beta_n^{(2)} - \beta_n^{(1)})$ for $\alpha_n^{(1)} = \alpha_n^{(2)} = \alpha_n$. Furthermore, assuming the first harmonic component is chosen for beamforming, by using $\beta_n^{(2)} - \beta_n^{(1)} = 1/2$, the $B_{n,1}$ (20) reduces to $\frac{2}{\pi}\sin(\pi\alpha_n)$, which results the maximum amplitude $B_{n,1}$. Additionally, the term $\frac{2}{\pi q}\sin(q\pi\alpha_n)\sin q\pi(\beta_n^{(2)} - \beta_n^{(1)})$ becomes zero for even harmonics because $\sin(u\pi/2)$ is always zero for even value of u. This concludes the reduction of harmonics and enables more power in the desired sideband. On the other hand, recalling that $\sin(.)$ is increasing function in $[0, \pi/2]$, by increasing α_n, the term $\frac{2}{\pi q}\sin(q\pi\alpha_n)$ increases for low order harmonics most. This results in an increased gain or reduced SLL at the low-order harmonics. Hence, the low-order harmonics of the alternating switching are used for beamforming by controlling the switching parameters. As can be shown in (21), the α_n determines the strength of the AF and hence, the shape, SLL, and the desired/undesired SBs. We consider (28) to beamform the desired harmonic component. Therefore, alternating switching and the proposed analytical reasoning are ideal for NTN-UT applications.

Showing the significance of the alternating switching, for the sake of clarity, we present the subsequent works based on 'simple' on-off switching. Extending to alternate switching can be easily addressed based on Section A (A), and we kept it for future work.

The majority of the literature relies on a fixed switching sequence. Other researchers apply meta-heuristic algorithms, [37], to determine α_n and β_n which neither guarantees the optimal solution nor is economical in computing resources. Maintaining directivity while decreasing SLL was hardly achievable in the phased array with the same aperture size or low-cost algorithms. This paper formulates a quadratic optimization problem and optimizes the switching parameters to suppress the SLL with stringent directivity requirements. We represent the directivity using the First Null BeamWidth (FNBW) (Ω), and we can define it as twice the angular difference between the peak of the main lobe and the first null. Mathematically,

$\Omega = 2|\{\arg\max_\theta |AF(\theta)| - \arg\min_{\theta'} |AF(\theta)|\}|$, where $\theta', \theta \in [0, \pi]$ and $\theta' \neq \theta$. Here, we consider $\theta < \theta' < \tilde{\theta}$ so that the first null is between the main lobe and the SLL, θ is the main lobe index, and $\tilde{\theta}$ refers to the maximum SLL index as given in (32). Alternatively, we set the time-independent part of the AF (8) to 0 for the first harmonic component as $\sum_{n=0}^{N-1}\alpha_n \operatorname{sinc}(\pi\alpha_n)e^{-j\pi(\alpha_n+2\beta_n)}e^{jnkd\cos(\theta)} = 0$ and we solve for θ numerically. A numerical iterative method is used to compute the FNBW as shown in Algorithm 1. The FNBW depends on the aperture size in ULA, but in TMA, it also depends on α_n and β_n with the time additional degree of freedom. Chebyshev tapering assigns higher amplitudes to central elements and lower to edge elements, reducing the SLL at the expense of the beamwidth. Since TMA is time-based (not amplitude-based) modulation, it does not change the effective aperture of the array or physical arrangement of elements, which enables SLL reduction with insignificant changes in beamwidth. Since the SLL and beam shape strongly determine the SINR and beamforming performance, we formulate a joint SLL and FNBW optimization. With the SLL given in (32), we formulate the SLL and FNBW as a multi-objective optimization problem as:

$$\begin{aligned}&\min_{\alpha_n,\beta_n}\{SLL + \Omega\},\\ s.t. \quad &c_1 : \beta_n = \frac{1}{2}[n\cos\theta - \alpha_n],\\ &c_2 : 0 \leq \alpha_n \leq 0.5,\\ &c_c : \max_\theta |AF(\theta, t)|^2 = 1,\end{aligned} \tag{34}$$

where Ω is the FNBW, SLL is the maximum SLL (32), and $|AF(\theta, t)|^2 = 1$ indicates the maximum normalized gain of the antenna response in the DoA θ. The optimization problem (34) is formulated as a Quadratic Programming Optimization (QPO), which is a non-convex problem. While the objective function is a joint SLL and FNBW optimization as a function of TMA switching parameters,

we start the optimization by initializing the optimization variables. The TMA switching delay, c_1, is primarily used for beam steering and is initialized as $[0, 0.25]$. We initialize the switching pulse duration α_n of c_2, within the lower and upper bounds, a_{lb} and a_{ub}, respectively. The constraint c_3 of (34) indicates that the array response is normalized. Then, we set the initial values for the step size μ and tolerance γ algorithm parameters. We use a standard iterative optimization tool, quadratic programming, to solve the problem. The solver is known for its almost global solution, but since the problem is non-linear, the solution can also converge to a local minimum. On the other hand, despite its robustness, the design of the TMA switching parameters using QPO depends on the accuracy and availability of the DoA. The details of the QPO are given in Algorithm 1.

Algorithm 1 SLL and FNBW optimization

Input: DoA, N, a_{lb}, a_{ub}
Output: $a_{\text{opt}}(\alpha_n, \beta_n)$, SLL, Ω
Initialize $a_n \in [a_{\text{lb}}, a_{\text{ub}}]$, μ, γ
function OBJECTIVE FUNCTION(a_n, N)
    Calculate SLL and Ω from the AF
    return SLL(α_n) + $\Omega(\alpha_n)$
end function
$a_{\text{opt}} = \text{fmincon}(\text{Objective Function}, a_n, a_{\text{lb}}, a_{\text{ub}})$
function $\Omega(\alpha_n)$
    $[V, M] \leftarrow \max(AF), r \leftarrow M, f \leftarrow M$
    while $AF(r) > AF(r+1)$ **do**
        $r \leftarrow r + 1$, right side 1^{st} null index
    end while
    while $AF(f) > AF(f-1)$ **do**
        $f \leftarrow f - 1$, left side 1^{st} null index
    end while
    $\Omega \leftarrow [\theta(r) - \theta(f)] \times \frac{180}{\pi}$
end function

For the same problem (34), we included the Particle swarm optimization (PSO) algorithm to solve the multivariate problem. The PSO is a well-known algorithm based on simple individual interactions that can lead to complex global behaviour. The principle is simple; we randomly generate the positions and velocities of every particle in the search space, with the particle's personal best (pBest) as its initial position and a global best (gBest) position. Then, we evaluate the fitness of every particle using the objective function (SLL and FNBW). Next, we update pBest if the current position's fitness is better than its previous pBest and gBest to the best position any particle finds. Finally, the particle's velocity, which includes cognitive and social coefficients and the position, is updated until the end of the iteration. We adopt the formulation of PSO based on [38], [39], and [40].

B. ADAPTIVE BEAMFORMING USING IMPERFECT DoA

Due to the dynamics of the LEO satellite, adaptive beamforming is fundamental to continuously adjusting to changing conditions. We introduce ADMM and ASPC beamforming based on a beacon signal $d(t)$ as shown in Fig. 4.

1) TMA beamforming design using ADMM

We propose a BF design where an NTN-UT receives a signal transmitted from a LEO satellite downlink. The beamforming employs a training signal $d(t)$ to adaptively design the TMA switching parameters without needing pre-defined DoA information, as shown in Fig. 4. From (15), for $q = 1$, the steering vector $a_n(\theta)$ and the Fourier series coefficient of the TMA w_n are $e^{jnkd\cos\theta}$ and $1/\pi.\sin(\pi\alpha_n)e^{-j\pi(\alpha_n+2\beta_n)}$, respectively. Recall that $x_n(t) = h_n c(t)$ and $n = 0, 1, ..., N-1$, we can rewrite (15) as:

$$y(t) = \mathbf{w}^T[\mathbf{x}(t) \odot \mathbf{a}(\theta)] + \eta(t), \mathbf{w}, \mathbf{x}(t), \mathbf{a}(\theta) \in \mathbb{C}^{N\times 1} \quad (35)$$

where, $\odot$ is Hadamard product, $\mathbf{w} = [w_0, w_1, \cdots, w_{N-1}]^T$, $\mathbf{a}(\theta) = [a_0(\theta), a_1(\theta), \cdots, a_{N-1}(\theta)]^T$, and $\mathbf{x}(t) = [x_0(t), x_1(t), \cdots, x_{N-1}(t)]^T$. The $t = 1, \cdots, T$ is the discrete sampling instant with $T > N$. Assuming $h_n = 1$, we formulate the problem as a mean square error minimization:

$$\min_{\boldsymbol{\alpha}, \mathbf{a}(\theta)} \mathbb{E}[\|d(t) - y(t)\|^2], \quad (36a)$$

$$s.t. \quad c_1 : \beta_n = \frac{1}{2}[n\cos\theta - \alpha_n], \forall n \quad (36b)$$

$$c_2 : 0 \le \alpha_n \le 0.5, \quad (36c)$$

$$c_3 : 0 \le \theta \le \pi. \quad (36d)$$

The ADMM is a robust parallel optimization algorithm that divides the problem into sub-problems. Accordingly, we reformulate the problem $J = \mathbb{E}\left[\|d(t) - y(t)\|^2\right]$ using ADMM as an augmented penalized Lagrangian as:

$$L_\rho(\alpha_n, \theta, \beta_n, \lambda_n) = \mathbb{E}\left[\|d(t) - y(t)\|^2\right] + \lambda_n[\frac{1}{2}(n\cos\theta - \alpha_n) - \beta_n] + \frac{\rho}{2}[\frac{1}{2}(n\cos\theta - \alpha_n) - \beta_n]^2, \quad (37)$$

where λ_n is the n^{th} Lagrangian multiplier and ρ is the penalty parameter of the augmented Lagrangian. To solve the problem, we design the update rules of $\alpha_n, \beta_n, \theta$, and λ_n as follows:

- **Update of** α_n: First, we differentiate L_ρ $w.r.t$ α_n.

We have, $\frac{\partial}{\partial\alpha_n}J = -2\mathbb{E}[(d(t) - y(t))\frac{\partial y(t)}{\partial\alpha_n}]$ and $\frac{\partial y(t)}{\partial\alpha_n} = \frac{\partial \mathbf{w}^T}{\partial\alpha_n}[\mathbf{x}(t)\odot\mathbf{a}(\theta)]$. We have $\frac{\partial w_n}{\partial\alpha_n} = e^{-j2\pi(\alpha_n+\beta_n)}$ and hence:

$$\frac{\partial}{\partial\alpha_n}J = -2\mathbb{E}[[d(t) - y(t)]\frac{\partial w_n}{\partial\alpha_n}[x_n(t)a_n(\theta)]] \quad (38)$$

By including gradients of the second and third terms of L_ρ:

$$\nabla_{\alpha_n}L_\rho = \frac{\partial}{\partial\alpha_n}J - \frac{1}{2}\lambda_n + \frac{\rho}{2}[\beta_n - \frac{1}{2}(n\cos\theta - \alpha_n)]. \quad (39)$$

By setting (39) to 0 and solving for α_n, we update α_n as:

$$\alpha_n^{l+1} = \frac{-8}{\rho}\mathbb{E}\left[[d(t)-y(t)]\, e^{-j2\pi(\alpha_n+\beta_n^l)} x_n(t)a_n(\theta^l)\right] + 2\beta_n + \frac{n\cos\theta^l}{2} - \frac{2\lambda_n^l}{\rho},\ l = 1, 2, \ldots \text{ is the iteration.} \tag{40}$$

In general, the α_n update can be formulated as:

$$\alpha_n^{l+1} = \arg\min_{\alpha_n} L_\rho(\alpha_n, \theta^l, \beta_n^l, \lambda_n^l), \tag{41}$$

- **Update of θ:** First, we differentiate the steering vector as $\frac{\partial}{\partial\theta}a_n(\theta) = -jnkd\sin\theta a_n(\theta)$. Next, we differentiate the second and third terms of L_ρ as $-\frac{1}{2}\boldsymbol{\lambda}^T\mathbf{n}\sin\theta$ and $-\frac{\rho}{2}\left(\boldsymbol{\beta} - \frac{1}{2}(\mathbf{n}\cos\theta - \boldsymbol{\alpha})\right)^T\mathbf{n}\sin\theta$, respectively, where $\boldsymbol{\lambda} = [\lambda_0, \lambda_1, ..., \lambda_{N-1}]$ and $\mathbf{n} = [0, 1, ..., N-1]$. Then:

$$\nabla_\theta L_\rho = -2\mathbb{E}[(d(t)-y(t))\mathbf{w}^T[\mathbf{x}(t)\odot\frac{\partial}{\partial\theta}\mathbf{a}(\theta)]] - \frac{1}{2}\boldsymbol{\lambda}^T\mathbf{n}\sin\theta + \frac{\rho}{2}[\boldsymbol{\beta} - \frac{1}{2}(\mathbf{n}\cos\theta - \boldsymbol{\alpha})]^T\mathbf{n}\sin\theta. \tag{42}$$

Setting (42) to 0, we can solve θ numerically as:

$$\theta^{l+1} = \arccos\{[\frac{4}{\rho\mathbf{n}^T\mathbf{n}}(2jnkd\mathbb{E}[(d(t)-y(t))y(t)] - \frac{1}{2}\boldsymbol{\lambda}^{l^T}\mathbf{n} + \frac{\rho}{2}\boldsymbol{\beta}^{l^T}\mathbf{n} + \frac{\rho}{4}\mathbf{n}^T\boldsymbol{\alpha}^{l+1})]\} \tag{43}$$

Using α_n^{l+1} value from (41), we formulate θ update as:

$$\theta^{l+1} = \arg\min_{\alpha_n} L_\rho(\alpha_n^{l+1}, \theta, \beta_n^l, \lambda_n^l), \tag{44}$$

- **Update of β_n:** Similar to the procedure in α_n, we derivate $\frac{\partial w_n}{\partial\beta_n}$ as $-2j\pi\frac{\sin(\pi\alpha_n)}{\pi}e^{-j\pi(\alpha_n+2\beta_n)}$ and $\frac{\partial}{\partial\beta_n}J$ is $\mathbb{E}[-2\text{Re}((d(t)-y(t))x_n(t)a_n(\theta)\frac{\partial w_n}{\partial\beta_n})]$. Therefore, the gradient of the augmented Lagrangian with β_n is:

$$\nabla_{\beta_n}L_\rho = \frac{\partial}{\partial\beta_n}J + \lambda_n + \rho[\beta_n - \frac{1}{2}(n\cos\theta - \alpha_n)] \tag{45}$$

We can compute β_n by setting (45) to 0. Alternatively, we can approximate β_n using the steering formula as:

$$\beta_n^{l+1} = \frac{1}{2}(n\cos\theta^{l+1} - \alpha_n^{l+1}) \tag{46}$$

- **Update of λ:** Since $\frac{\partial}{\partial\lambda_n}J = 0$, λ_n update is:

$$\lambda_n^{l+1} = \lambda_n^l + \rho[\beta_n^{l+1} - \frac{1}{2}(n\cos\theta^{l+1} - \alpha_n^{l+1})]. \tag{47}$$

Hence, ADMM results in 4 equations and 4 variables, and we solve it iteratively as is summarized in Algorithm 2.

In the initialization, $\boldsymbol{\alpha}^0$ is a random initial value of the pulse duration $\in [0, 0.5]$, similarly $\boldsymbol{\beta}^0 \in [0, 0.25]$ based on (27) is the initial value of the switching delay, $\theta^0 \in [0, \pi]$ is the initial guess of the DoA, $\boldsymbol{\lambda}^0$ is the initial of the Lagrangian multiplier, ρ is the penalty parameter, l_{max} is the maximum iteration, and N is the number of elements. Algorithm 2 outputs the optimal TMA switching parameters, $\boldsymbol{\alpha}$ and $\boldsymbol{\beta}$, and the optimal DoA.

Algorithm 2 TMA beamforming design using ADMM

Initialize: $\boldsymbol{\alpha}^0$, $\boldsymbol{\beta}^0$, θ^0, $\boldsymbol{\lambda}^0$, ρ, l_{max}, N, $n \leftarrow 0$, $l \leftarrow 0$
while $l < l_{max}$ **do**
  for each $n < N$ **do**
    Update α_n^{l+1} (41), θ^{l+1} (44), β_n^{l+1}, λ_n^{l+1} (47)
    Project α_n^{l+1} to (36c) and θ^{l+1} to (36d)
    $n \leftarrow n + 1$
  end for
  $l \leftarrow l + 1$
end while
Output: Optimal $\boldsymbol{\alpha}$, $\boldsymbol{\beta}$, DoA

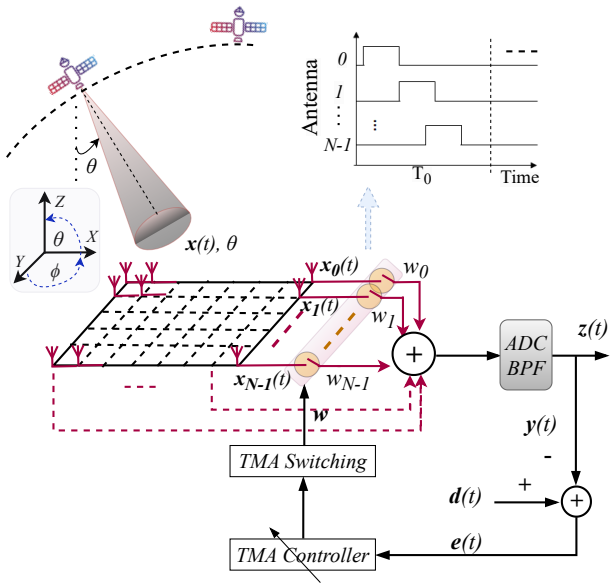

Figure 4: Downlink beamforming at the NTN UT using a beacon signal (ADMM and ASPC methods)

2) TMA beamforming design using ASPC

Similar to the ADMM method, we formulate the receiving beamforming as detailed using the steepest descent concept:

$$\min_{\mathbf{w},\mathbf{a}(\theta)} \mathbb{E}[||d(t)-y(t)||^2] \text{ s.t. (36b) - (36d)} \tag{48}$$

By representing (48) as $J = \mathbb{E}[e^2(t)]$, where $e(t) = d(t) - \sum_{n=1}^{N} w_n x_n(t) a_n(\theta)$, the minimum error occurs when $\frac{\partial J}{\partial \mathbf{w}}$ is set to 0. However, since $\mathbf{w}$ depends on α_n, $\frac{\partial J}{\partial \mathbf{w}}$ cannot be differentiated directly. So, to differentiate it $w.r.t$ α_n, using the chain rule, we have $\frac{\partial J}{\partial \alpha_n} = -2\mathbb{E}[e(t)\frac{\partial e(t)}{\partial \alpha_n}]$. Since $x_n(t)$ and $a_n(\theta)$ are independent of α_n, using $\frac{\partial w_n}{\partial \alpha_n} = e^{-j\pi(\alpha_n+2\beta_n)}[\cos(\pi\alpha_n) - j\sin(\pi\alpha_n)]$, we have:

$$\frac{\partial J}{\partial \alpha_n} = -2\mathbb{E}[e(t)x_n(t)a_n(\theta)e^{-j\pi(2\alpha_n+2\beta_n)}] \tag{49}$$

Note that $\frac{\partial w_n}{\partial \alpha_n}$ can be represented as $\cos(\pi\alpha_n)e^{-j\pi(\alpha_n+2\beta_n)} - j\pi w_n$. Finally, by equating

(49) to 0 and solving $\mathbf{w}$, we formulate the problem as:

$$\mathbf{w}^{l+1} = \mathbf{w}^{l} + \mu \nabla J(\mathbf{w}), \text{ where } \mu \in [0.1, 1] \text{ is step size.} \tag{50}$$

However, the steepest descent requires expensive gradient computation, a burden to the NTN-UT. Hence, we propose an instantaneous square error minimisation using the Least Mean Square (LMS) algorithm as:

$$\mathbf{w}^{l+1} = \mathbf{w}^{l} + \mu e(t)[\mathbf{x}(t) \odot \mathbf{a}^{l}(\theta)] \tag{51}$$

To compute (51), we divide the problem into several sequential iterations. Firstly, we compute the l^{th} iteration $\boldsymbol{\beta}^{l}$ using the l^{th} initial value of $\boldsymbol{\alpha}$ and θ based on (26) as:

$$\boldsymbol{\beta}^{l} = [\mathbf{n}\cos\theta - \boldsymbol{\alpha}^{l}]/2. \tag{52}$$

Next, we compute $\mathbf{a}^{l}(\theta)$ from DoA θ, which also enables us to compute $\mathbf{w}^{l+1}$. Finally we update $\boldsymbol{\alpha}^{l+1}$ from $\mathbf{w}^{l+1}$ as:

$$\boldsymbol{\alpha}^{l+1} = \mathrm{Re}\{\frac{1}{\pi}\sin^{-1}[\pi \mathbf{w}^{l+1} e^{j\pi(\boldsymbol{\alpha}^{l}+2\boldsymbol{\beta}^{l})}]\}. \tag{53}$$

Using the optimal $\mathbf{w}$ and $\mathbf{a}(\theta)$, we can extract the signal as:

$$z(t) = \mathbf{w}^{T}[\mathbf{x}(t) \odot \mathbf{a}(\theta)]. \tag{54}$$

To summarise, with the ADMM method, the gradient computation and the decomposition of the problem enable a likely global solution. The ASPC technique, as outlined in Algorithm 3, computes the design variables based on the instantaneous error. The instantaneous error is evaluated against a predefined error threshold, and the result is used to decide if the estimated signal agrees with the training signal. When the error is less than the threshold, the algorithm assumes both the TMA design parameters, α_n and β_n, and the DoA are optimal. ASPC is designed with fewer design variables than ADMM, making it ideal for real-time satellite tracking and low-cost systems like NTN UT. In the proposed scenario, the optimization speed and channel state information are critical. Hence, the ASPC and ADMM are proposed for their low computational complexity and potentially lower power consumption.

Algorithm 3 TMA beamforming design using ASPC

Input: $v_r, d(t), N, d$
Output: $\alpha_n, \beta_n, \theta$
Initialization: $\mathbf{w}$, μ, l_{max}, threshold ϵ, DoAs i_{max}

for $DoA = \theta_i,$ where, $i = 1, 2, \ldots, i_{max}$ **do**
  for iteration, $j = 1, 2, \ldots, l_{max}$ **do**
    Calculate $\mathbf{a}^{l}(\theta) = e^{j\mathbf{n}kd\cos\theta_i}$
    Estimate signal $y(t) = \mathbf{w}^{T}(\mathbf{x}(t) \odot \mathbf{a}^{l}(\theta))$
    Compute error: $e(t) = d(t) - y(t)$
    if $|e^{2}(t)| > \epsilon$ **then**
      Update $\mathbf{w}^{l+1}$ from $e(t)$ and $\mathbf{a}^{l}(\theta)]$ using (51)
      Update $\boldsymbol{\alpha}^{l+1}$ from $\mathbf{w}^{l+1}$ using (53)
    end if
  end for
  Extract signal $z(t) = \mathbf{w}^{T}[\mathbf{x}(t) \odot \mathbf{a}(\theta)]$ using (54)
  DoA $\leftarrow \theta_i$
end for

V. NUMERICAL RESULTS

In this paper, we study NTN-UT receiving beamforming design in satellite systems. We assume the LEO satellite transmits to an NTN-UT as usual in the downlink, and the UT is equipped with TMA. We consider the LEO satellite system given by 3GPP Rel.16 technical specification of NR that supports NTN, shown in Table I.

Table I: *Evaluation parameters*

Parameter	Symbol	Setting
Orbital height	H	600 km
$3dB$ beamwidth	Ω	4.4°
Carrier frequency	f_c	2 GHz
UT receiver gain	G_r	0 dB
Noise bandwidth	B	30 MHz
Reference Temperature	T	290 k
Boltzmann's constant	K	$1.23x10^{-23}$
Satellite EIRP	E_r	34 dBW/MHz

A. COMPARISON OF ULA AND TMA-BASED BEAMFORMERS

First, to compare the cost and complexity of ULA and TMA, we use the number and type of components, number of beams, gain, beamwidth, and beamforming network (BFN) parameters. To evaluate the NTN UT beamforming, the ULA, conventional TMA, and Tapered TMA are compared as shown in Fig. 5. For the same aperture size, comparing ULA and TMA, TMA realizes multiple beams in a single RF-Front end, which is important for handover and multi-satellite connections. The TMA beams are also more directive than the ULA beams. With ULA, multiple beams are possible only with multiple RF-Front ends or at the expense of complex BFNs. The aperture size of the ULA has to increase to generate a beam as directive as a TMA beam. Due to the phase shifters, increased aperture size, or complex BFNs, ULA is expensive to implement in NTN UTs. However, conventional TMA beams have a lower gain than ULA. As shown in Fig. 5 in dotted lines, we Tapered both ULA and conventional TMA using the Chebyshev method. Tapering reduces the SLL significantly and decreases directivity and gain, indicating that tapering incurs additional costs and complexity in enhancing performance.

B. TMA SINR PERFORMANCE ANALYSIS

To study the SINR impact of TMA, we designed the downlink channel model based on the details given in [33]. A multi-beam LEO satellite is assumed to be located at the Earth-Centred-Earth-Fixed reference (ECEF) of $6,978,140$ km, and its latitude and longitude are located in central Europe, $49.8^{\circ}N, 6.13^{\circ}E$. We consider a seven-beam scenario in which a UT is located at the centre of the central beam, and the other six beams uniformly encircle it in 2D. The six

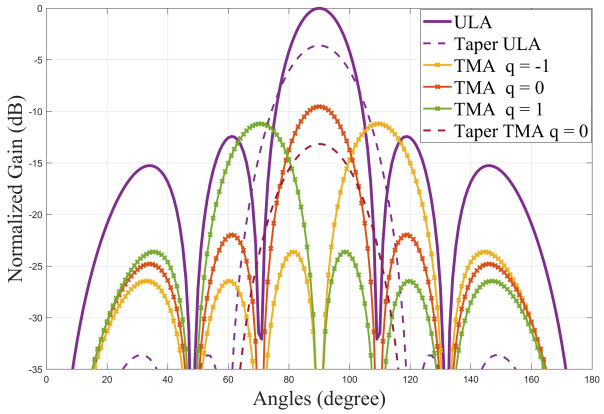

Figure 5: ULA, TMA, and Taper performances

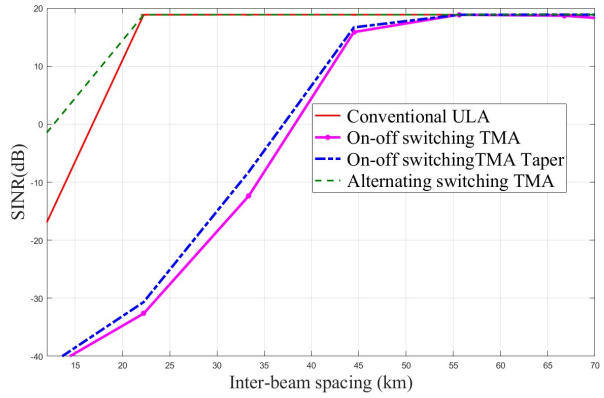

Figure 6: SINR comparison using ULA, conventional TMA, and alternating switching TMA

beams introduce interference to the user served by the central beam. We compare the SINR of the conventional array and both TMA switching schemes for the same beamwidth as shown in 6. From Fig. 6, we can observe that the ULA and alternating switching TMA outperform the rest of the TMAs, followed by tapered TMAs. Because we use the same beamwidth, the SINR performance difference is mainly due to the gain performance difference. Considering the cost and complexity, ULA is characterized by expensive phase shifters. Despite its low cost, the conventional TMA is the worst in gain and SINR. Even though the tapering enables higher SLL than the conventional TMA, to compensate for the beamwidth, we increase the number of elements, which increases cost and complexity. The alternating switching performs almost the same as ULA, making it the most promising solution for low-cost NTN-UTs with more details quantified in Table III.

C. IMPACT OF ARRAY SIZE ON IMPERFECT CHANNEL

Assuming the satellite signal is modulated by Binary Phase Shift Keying (BPSK), the UT equipped with TMA receives the signal under AWGN. We studied perfect and imperfect DoA beam alignments. We use ideal alignment and a 2° misalignment. Finally, $100,000$ bits are transmitted, and the Bit Error Rate (BER) is evaluated for a range of SNR, as shown in Fig. 7. We use a different number of elements

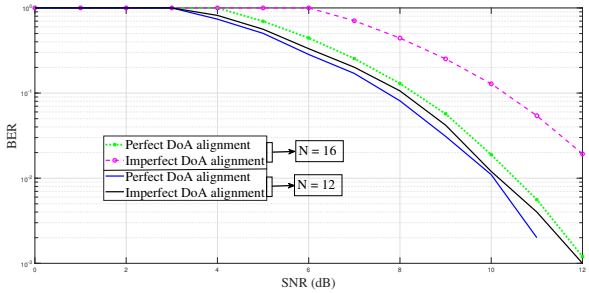

Figure 7: Channel estimation response

N to evaluate the BER sensitivity, as shown in Fig. 7. In both cases, the perfect alignment outperforms slightly, giving room for channel imperfection, which depends on the N.

D. UPA AND 2D TMA SWITCHING DESIGN COMPARISON

The gain of 4×4 UPA and conventional TMA (in 2D structure) is shown in Fig. 8(a) and Fig. 8(b), respectively. The gain of the unavoidable fundamental component dominates the SBs when α_n increases in the conventional TMA. Additionally, when α_n decreases, we have many low-gain SBs. However, the fundamental component is not used for beamforming. From Figures 8(a) and 8(b), the gain of conventional TMA is lower than ULA.

A typical plot of alternating switching with 0.25 of α_n is shown in Fig. 8(c) for the same aperture size as UPA Fig. 8(a). The gain with the alternating switching has significantly increased over the same aperture of the conventional TMA. By reducing α_n to 0.1, we can easily increase the number of beams as shown in Fig. 8(d). This increase in the number of beams, of course, reduces the gain. However, unlike the conventional TMA, the gain increases with the number of elements in the alternating switching scheme, similar to UPA.

By increasing the array size to 8×8 elements and employing alternating switching, we synthesize 2 beams with the gain per beam surpassing that of the phased array. The resulting beams are also focused compared to the 4×4 TMA or 4×4 phased array. Using UPA with a linear BFN of 32 elements, generating 2 beams with the same gain as the alternating switching TMA is possible. However, additional costs and complexity are mandatory to shape the beams on top of the 32 phase shifters' costs. Hence, compared to the phased array, TMA with alternating switching is a promising replacement for NTN UT while leveraging low implementation cost and complexity. Additional details of

This article has been accepted for publication in IEEE Open Journal of the Communications Society. This is the author's version which has not been fully edited and content may change prior to final publication. Citation information: DOI 10.1109/OJCOMS.2024.3522519

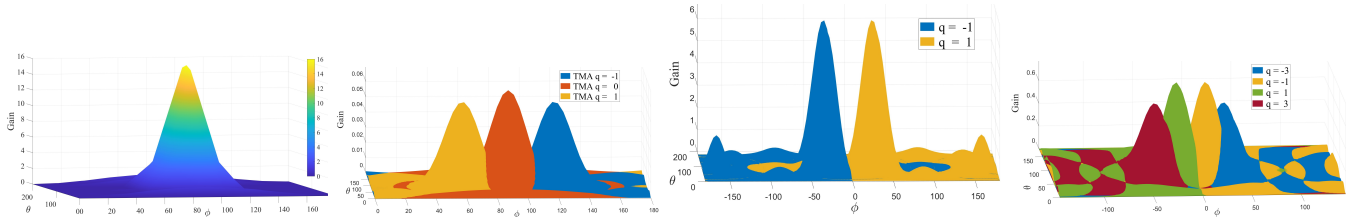

(a) Conventional array: 1 beam (b) Single-pulse switching: 3 beams (c) Alternating switching: 2 beams (d) Alternating switching: 4 beams

Figure 8: Cost, complexity, and performance comparisons of UPA and TMA beamforming

the cost, complexity, and performance comparisons are given in Table III.

E. DYNAMIC BEAMFORMING USING OPTIMIZATION

Using the first harmonic component, we simulate the optimal result of the joint SLL/gain and beamwidth optimization as shown in Fig. 9. For $\lambda/2$ inter-element spacing, we use a quadratic programming optimization (QPO) solver $Fmincon$ in Matlab and the optimal design results in significant SLL reduction over the traditional α_n fixed at $1/N$. Additionally, we have included the conventional PSO for the same objective function as QPO. The PSO optimises the TMA switching pulse duration with 20 particles, 100 iterations, 0.5 inertia, and 1.5 social and cognitive parameters while minimizing the SLL and FNBW. The performance of PSO depends on the choice of the optimization parameters, which is not easy. Hence, QPO has shown superiority in SLL reduction. Unlike the Chebyshev method, the QPO enables the SLL reduction with negligible beamwidth damage. The fixed and optimized switching sequences, shown in Table II, result in significant TMA performance differences.

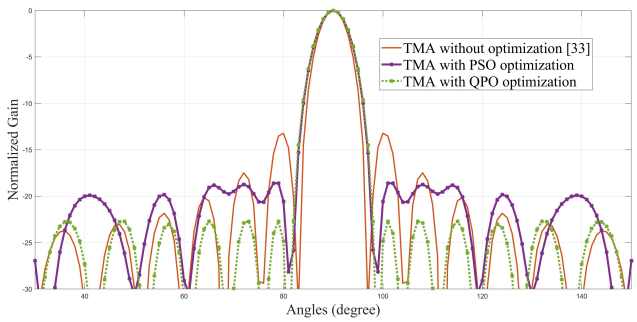

Figure 9: Comparison of gain/SLL and beamwidth of (i) TMA with and without optimization, and (ii) TMA and PSO

F. ADAPTIVE BEAMFORMING USING ADMM AND ASPC

The orbital speed and orbital period are calculated by assuming a circular orbit of 600 km height LEO satellite and 2 GHz operating frequency to compare the QPO, ADMM, and ASPC methods. Then, the time taken for the satellite to cover DoA angles is calculated. The QPO

Table II: *TMA switching sequences*

Method	TMA switching pulse duration, α_n
TMA [33]	1/N 1/N 1/N 1/N 1/N 1/N 1/N 1/N 1/N 1/N 1/N 1/N 1/N 1/N 1/N
TMA with PSO	0.4161 0.2427 0.1995 0.1995 0.2088 0.2727 0.3729 0.3357 0.3568 0.2820 0.2381 0.3849 0.1106 0.1561 0.0827 0.0889
TMA with QPO	0.1855 0.1274 0.1673 0.2072 0.2462 0.2864 0.3203 0.3355 0.3355 0.3203 0.2864 0.2462 0.2071 0.1673 0.1274 0.1855

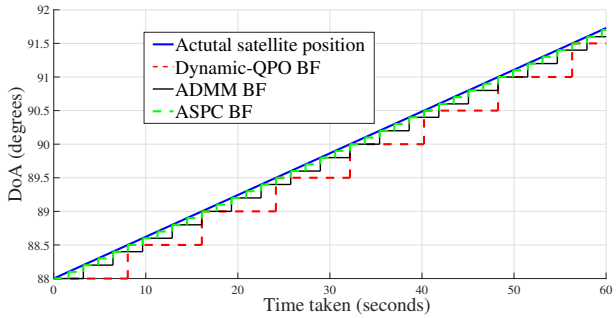

Figure 10: Comparisons of dynamic (QPO), ADMM, and ASPC methods of beamforming designs

design updates slowly because of its computing-intensive optimization. The QPO method requires perfect DoA, which is neither easy nor fast. For the NTN UT communicating with fast mobility LEO satellite, the slow response of QPO challenges the implementation of the BF, as shown in Fig. 10. On the other hand, the ADMM and ASPC methods adaptively estimate the optimal TMA parameters and DoA while leveraging fast-tracking. The results indicate that the DoA of ASPC is closer to the true satellite DoA because of its fast response than ADMM, as shown in Fig. 10. In fact, the ASPC can converge to local optima because of the non-linear objective function, especially with inappropriate initialization. In ADMM, the problem is split into subproblems, which exhibit reduced complexity or even convexity and are potentially resilience against local minima.

Complexity-wise, channel conditions, such as the DoA, change fast since the LEO satellite moves at high speed. In the NTN system, satellites periodically transmit their ephemeris data (orbital information), and the NTN UT approximates the azimuth and elevation angle based on its coordinates relative to the satellite's coordinates, providing an initial DoA. The proposed QPO works based on a predefined DoA, which relies on a separate DoA computation, increasing response time and complexity. In ADMM and ASPC, the DoA is estimated adaptively from the beacon signal, reducing DoA update complexity. Additionally, since ADMM and ASPC work based on mathematical simplification, they are generally light in complexity. Comparing ADMM and ASPC, the ADMM relies on gradient computation and introduces an intermediate variable, making it more complex than ASPC. The ASPC works based on the Least Mean Square (LMS) algorithm, which is relatively light in complexity. The cost function is non-convex; hence, the ASPC may converge to local minima depending on the selection of initial variables. QPO enables reliable solutions mainly because it works based on predefined DoA. Generally, QPO relies on DoA availability and slow convergence speed. However, the optimization speed and channel state information are critical in satellite systems. Hence, while the significance of QPO is not trivial, ADMM and ASPC are highly recommended in the proposed scenario. Due to its gradient computation and decomposition of the problem into simpler subproblems, the ADMM enables almost a global solution compared to ASPC. For cost reasons, algorithms with low computational complexity, such as ADMM and ASPC, sound ideal for the proposed NTN UT scenario.

Regarding the channel state information update, for a known operating height, we determine the orbital velocity and period from the operating frequency, gravitational constant, and mass and radius of Earth using the circular orbit of orbital speed equation, [41], [42]. Consequently, we can compute coherence time and Doppler spread parameters to determine some of the channel information update frequency. Generally, the update of LEO satellite constellations' orbital information varies depending on the satellite's mission. Starlink and OneWeb LEO satellites typically update their orbital information every few seconds. Considering the speed of LEO satellites, the channel state information updates from milliseconds to seconds based on 3GPP 22.261 (Rel 18). In line with this, the proposed algorithms update from a fraction of a second (ASPC) to a few seconds (QPO).

G. SUMMARY OF TMA BEAMFORMING COST, COMPLEXITY, AND POWER CONSUMPTION ANALYSIS

Even though the concept of cost and complexity considers a wide range of components and BFNs, the elements that significantly impact it are summarized in Table III. The performance and cost/complexity of the alternating switching TMA and UPA are compared (both in 2D structure). As shown in the first and second rows of Table III, we have 04 beams using a linear BFN of UPA and the same number of beams are synthesized using TMA with a single RF-front end. On top of the cost and complexity due to the increased number of elements, the UPA induces significant cost and complexity due to the increased number of phase shifters. While TMA enables focused beams, ideal for NTN UT, the UPA incurs additional costs to reduce the beamwidth.

Table III: *Major cost and complexity analysis*

2D Array Structure	Number of Beams	Number of Elements	Number of Phase Shifters	Gain per Beam (dB)
UPA	04	64	64	16
TMA	04	16	01	01
UPA	02	32	32	16
TMA	02	36	01	14
TMA	02	49	01	20

However, TMA has a lower gain in this setting than UPA. In the third row of Table III, using 32 elements of UPA, we synthesize 02 beams with 16 dB per beam. In the fourth and fifth rows of Table III, using 36 and 49 elements of TMA, we synthesize 02 beams with 14 and 20 dBs per beam, respectively. Hence, with a few more elements, the gain per beam of TMA surpasses UPA. As a result, TMA can replace UPA, gaining significant cost and complexity reduction with the TMA.

On the other hand, we compare a typical optimal TMA design given in Fig. 9 and a phased array with every element connected for an entire period. From Fig. 9, the TMA consumes only 20% of power of the phased arrays. The increased power consumption of the phased arrays results in increased operational costs, especially for mobile or battery-powered applications.

Considering RF-receiver beamforming, we evaluate the power consumption of the conventional ABF, DBF, and TMA BF. The power consumption is proportional to the number of elements and beams and the nature of the Low Noise Amplifier (LNA), mixer, ADC, phase shifter, and signal processing power consumption. For millimetre-wave with LNA, mixer, ADC, phase shifters, and signal processing power consumption given in [43], [44], [45], [46], and [47], respectively, we compare the power consumption of the conventional phased array with the TMA. In ABFs, the exponential increase in complexity and size makes it impractical to generate multiple beams simultaneously. Besides, a DBF with a 1024-element phased array, working at 500 MHz bandwidth with 8-bit ADC, the DSP processes 8 Tbps per beam, and this demands a significant amount of power and about 4×10^{12} multiplications per second per beam, [48]. Since TMA switching consumes negligible power, the power consumption of the conventional arrays due to phase shifters alone results in significant power consumption over

This article has been accepted for publication in IEEE Open Journal of the Communications Society. This is the author's version which has not been fully edited and content may change prior to final publication. Citation information: DOI 10.1109/OJCOMS.2024.3522519

TMA, as shown in Fig. 11. To evaluate the advantage of

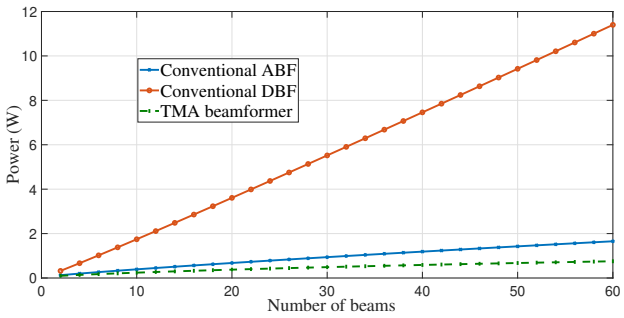

Figure 11: Power consumption of phased array and TMA

the TMA over the phase shifters, we compare the power consumption of the conventional phased array and the TMA, as shown in Fig. 12. We use the parameters considered from [43] to [47] and the phase shifters of the phased array replaced with the on-off switches. Accordingly, digital beamforming shows the worst power consumption, while analog beamforming consumes less power. From Fig. 12, it is evident that the TMA has considerable power consumption advantages over the conventional phased array-based analog and digital beamforming. Hence, the low cost, complexity, and power consumption make TMA ideal for NTN UT applications.

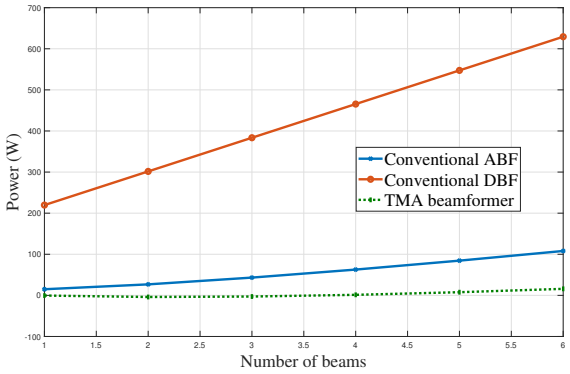

Figure 12: Per beam power consumption comparisons

In summary, comparing phased arrays and TMAs, phased arrays can easily adjust the phases across the array, making beam steering more straightforward. This enables fast and flexible communication of UTs with satellites. However, phase shifters are expensive to manufacture in addition to their power consumption, presenting challenges in commercial market penetration and multibeam scenarios. TMA employs a simple switching mechanism; hence, they are compact, cheap, and lightweight, which is critical for UTs. Table IV summarizes the pros and cons of the ABF and DBF of phased arrays and the TMA.

Table IV: Comparison summary of ABF, DBF, and TMA

Feature	ABF	DBF	TMA
Complexity	high (phase shifters)	Highest (more components)	Simplest (single RF)
Cost	Expensive (phase shifters)	Very expensive (ADC/DAC)	Cheapest (no phase shifters)
Beamforming resolution	Low (precision phase shifters)	Form and steer multiple beams	Good (time control)
Multiple beams	Not possible si-multaneously	Form at a time	Possible, signal process needed
Interference suppression	Limited	Best (precise control of elements)	Good, if SBs energy spread is engineered
Power consumption	High (phase shifters)	Very high (ADCs/DACs)	Least (on/off, single-RF)
Latency	Low	High	low

Regarding the suitability of the proposed beamforming solutions, it can be applied to TN UT and NTN UT. The impact of mobility is less critical for the TN UT, while the NTN UTs must adjust the direction of the beam to maintain consistent communication dynamically. The other issue is that the NTN links tend to be based on low received powers and direct paths, implying reliance on efficient beamforming to maintain SINR; this is not so critical in TN UT. Having said that, it is always preferable for the TN UT to be cost-efficient like NTN UT. This would imply low cost, low complexity, and low power consumption for the components, including beamforming. Hence, both the TN and NTN UTs share similar consumer requirements. Therefore, the proposed methodology can be applied to TN UTs as well. In fact, due to satellite mobility, doppler effects, and high path loss issues, the NTN UT demands stringent requirements.
In general, the proposed beamforming is suitable for UTs because it is low-cost, mainly due to the absence of phase shifters, compact due to simple hardware, precise in controlling the radiation pattern, and low-power consumption. Additionally, TMA enables multiple links using a single RF front end, potentially increasing spectral efficiency.
Lastly, multi-connectivity, well exploited in the Advanced Long Term Evolution (LTE-advanced), is rarely studied in the satellite industry [49]. Considering the speed of the LEO satellite and the TMA structure, we outline this research problem for future studies.

VI. CONCLUSION

In this work, we studied the beamforming performance, cost, and complexity of NTN UT using the conventional phased array, single-pulse switching, and alternating switching TMAs. The cost and complexity required to achieve a viable SINR are studied using different designs, yielding promising results with the alternating switching method.

We formulate and verify DoA to TMA switching parameters mapping equations to realise beam steering. To design efficient and low-cost NTN UT beamforming, we formulate multivariate nonlinear and multi-objective constrained optimization problems. Using quadratic programming and analytical methods, the beam shape, gain performance enhancements, and removal of unused harmonics are achieved for pre-defined DoAs. We introduce advanced TMA beamforming solutions based on a beacon signal using the ADMM and ASPC methods. The ADMM and ASPC methods have shown attractive adaptive iterative solutions, which is important in fast platforms like LEO satellites with UT communications. Finally, TMA's cost, complexity, performance, and power consumption are compared with the existing arrays, resulting in encouraging superiority with TMA, especially with the alternating switching. TMA is generally promising to NTN UT because of its dynamic beam-steering for satellite tracking and low-cost beamforming and interference suppression. The potential TMA beamforming for multi-link connectivity will be covered in future studies.

VII. APPENDIX A

To prove (20), recall that $j = e^{j\pi/2}$ and we need to prove $e^{-j\theta} - e^{-j\phi} = 2je^{-j(\theta+\phi)/2}\sin(\phi-\theta)/2$. Then, let $\theta = 2q\pi\beta_n^{(1)}, \phi = 2q\pi\beta_n^{(2)}$. Starting from the expression $e^{-j\theta} - e^{-j\phi}$ and factoring out this expression by $e^{-j\frac{\theta+\phi}{2}}$, the following holds true: $e^{-j\theta} - e^{-j\phi} = e^{-j\frac{\theta+\phi}{2}}[e^{-jx} - e^{jx}]$, where we let $x = (\theta-\phi)/2$ and $y = (\phi-\theta)/2$. Then, from Euler, we have $e^{j\theta} = \cos(\theta) + j\sin(\theta)$. Therefore, $e^{-jx} = \cos y - j\sin y$ and $e^{jx} = \cos x + j\sin x$. Subsequently, substituting this into the starting expression, we have $e^{-j\theta} - e^{-j\phi} = e^{-j\frac{\theta+\phi}{2}}[\cos y - j\sin y - \cos x - j\sin x]$. Since $y = -x$, we can simplify and combine like terms as, $e^{-j\theta} - e^{-j\phi} = 2je^{-j[(\theta+\phi)/2]}\sin y$ concludes the proof.

References

[1] A. Lappalainen and C. Rosenberg, "Can 5G Fixed Broadband Bridge the Rural Digital Divide," *IEEE Communications Standards Magazine*, vol. 6, no. 2, pp. 79–84, 2022.

[2] T. Ahmmed, A. Alidadi, Z. Zhang, A. U. Chaudhry, and H. Yanikomeroglu, "The Digital Divide in Canada and the Role of LEO Satellites in Bridging the Gap," *IEEE Communications Magazine*, vol. 60, no. 6, pp. 24–30, 2022.

[3] B. Di, L. Song, Y. Li, and H. V. Poor, "Ultra-Dense LEO: Integration of Satellite Access Networks into 5G and Beyond," *IEEE Wireless Communications*, vol. 26, no. 2, pp. 62–69, 2019.

[4] A. Sattarzadeh, Y. Liu, A. Mohamed, R. Song, P. Xiao, Z. Song, H. Zhang, R. Tafazolli, and C. Niu, "Satellite-Based Non-Terrestrial Networks in 5G: Insights and Challenges," *IEEE Access*, vol. 10, pp. 11 274–11 283, 2022.

[5] A. Eltohamy, M. Elkhouly, P. Große, M. Landmann, and G. Del Galdo, "Efficient Phased Array Radiation Pattern Evaluation for 5G and SatCom On-The-Move (SOTM) Applications," in *2023 17th European Conference on Antennas and Propagation (EuCAP)*, 2023, pp. 1–5.

[6] Y. C. Gang Li, Shiwen Yang and Z.-P. Nie, "A Novel Electronic Beam Steering Technique in Time Modulated Antenna Array," *Progress In Electromagnetics Research*, vol. 97, no. 0, pp. 391–405, 2009.

[7] 3GPP, "Solutions for NR to Support Non-terrestrial Networks (NTN)," *Technical Specification (TS) 38.821, 3rd Generation Partnership Project (3GPP), Version 16.0.0.*, vol. 16, no. 0, 2019.

[8] 3GPP., "Study on Narrow-Band Internet of Things (NB-IoT) / enhanced Machine Type Communication (eMTC) Support for Non-Terrestrial Networks (NTN))," *Technical Specification (TS) 38.821, 3rd Generation Partnership Project, Version 0.5.0.*, vol. 16, no. 0, 2021.

[9] 5G Automotive Association, "Evolution of vehicular communication systems beyond 5G." [Online]. Available: https://5gaa.org/evolution-of-vehicular-communication-systems-beyond-5g/ (Accessedon:May26,2024)

[10] G. D. M. L. Boccia, G. Amendola and G. Angiulli, "Phase-only synthesis of reconfigurable linear arrays with optimized power patterns," 2023. [Online]. Available: https://connectivity.esa.int/sites/default/files/01_1145_Boccia.pdf

[11] U. S. Technology, "Successful Demonstration of Scalable Phased Array SATCOM Terminal," 2023. [Online]. Available: https://www.unmannedsystemstechnology.com/2023/10/successful-demonstration-of-scalable-phased-array-satcom-terminal/

[12] S. Zhang, C. Guo, T. Wang, and W. Zhang, "ON–OFF Analog Beamforming for Massive MIMO," *IEEE Transactions on Vehicular Technology*, vol. 67, no. 5, pp. 4113–4123, 2018.

[13] S.-M. Moon, S. Yun, I.-B. Yom, and H. L. Lee, "Phased Array Shaped-Beam Satellite Antenna With Boosted-Beam Control," *IEEE Trans. Antennas Propag.*, vol. 67, no. 12, pp. 7633–7636, 2019.

[14] Q. Zhang, S. Feng, L. Fu, J. Wen, J. Ge, and J. Ma, "Design and Implementation of Adaptive Digital Beamforming Based on FPGA," in *2023 4th China International SAR Symposium*, 2023, pp. 1–7.

[15] A. K. Pandey, "Phased Array Antenna with Beamforming Network for 5G mmWave Communication System," in *2020 50th European Microwave Conference (EuMC)*, 2021, pp. 364–367.

[16] Y. Yamada, C. Z. Jing, N. H. Abd Rahman, K. Kamardin, I. I. Idrus, M. Rehan, T. Abd Latef, T. Abd Rahman, and N. Q. Dinh, "Unequally Element Spacing Array Antenna with Butler Matrix Feed for 5G Mobile Base Station," in *2018 2nd International Conference on Telematics and Future Generation Networks*, 2018, pp. 72–76.

[17] I. I. Idrus, T. A. Latef, N. K. Aridas, M. S. A. Talip, Y. Yamada, T. A. Rahman, I. Adam, and M. N. M. Yasin, "A low-loss and compact single-layer butler matrix for a 5G base station antenna," *PLoS ONE*, vol. 14, no. 12, p. e0226499., 2019.

[18] Q. Zeng, P. Y, L. Yin, H. Lin, C. Wu, F. Y, and S. Y, "Phase Modulation Technique for Harmonic Beamforming in Time-Modulated Arrays," *IEEE Trans. Antennas Propag.*, vol. 70, no. 3, pp. 1976–1988, 2022.

[19] L. Poli, P. Rocca, L. Manica, and A. Massa, "Handling Sideband Radiations in Time-Modulated Arrays Through Particle Swarm Optimization," *IEEE Trans. Antennas Propag.*, vol. 58, no. 4, pp. 1408–1411, 2010.

[20] G. Ni, Y. Song, J. Chen, C. He, and R. Jin, "Single-Channel LCMV-Based Adaptive Beamforming With Time-Modulated Array," *IEEE Antennas Wireless Propag. Lett.*, vol. 19, no. 11, pp. 1881–1885, 2020.

[21] F. Yang, S. Yang, L. Sun, Y. Chen, S. Qu, and J. Hu, "DOA Estimation via Sparse Signal Recovery in 4-D Linear Antenna Arrays With Optimized Time Sequences," *IEEE Transactions on Vehicular Technology*, vol. 69, no. 1, pp. 771–783, 2020.

[22] Z. Li, F. Yang, Y. C, S.-W. Qu, J. Hu, and S. Yang, "Wideband Receive Beamforming Based on 4-D Antenna Arrays With Postmodulation," *IEEE Antennas Wirel. Propag. Lett.*, vol. 21, no. 4, pp. 740–744, 2022.

[23] R. Maneiro-Catoira, J. C. Brégains, and L. Castedo, "Enhanced Time-Modulated Arrays for Harmonic Beamforming," *IEEE Journal of Selected Topics in Signal Processing*, vol. 11, no. 2, pp. 259–270, 2017.

[24] R. Maneiro-Catoira, J. Brégains, J. A. García-Naya, and L. Castedo, "Time modulated array controlled by periodic pulsed signals," in *2018 26th European Signal Processing Conference*, 2018, pp. 637–641.

[25] Y.-Q. Yang, H. Wang, and Y.-X. Guo, "A Time-Modulated Array With Digitally Preprocessed Rectangular Pulses for Wireless Power Transmission," *IEEE Trans. Antennas Propag.*, vol. 68, no. 4, pp. 3283–3288, 2020.

[26] G. Bogdan, K. Godziszewski, Y. Yashchyshyn, C. H. Kim, and S.-B. Hyun, "Time-Modulated Antenna Array for Real-Time Adaptation in Wideband Wireless Systems—Part I: Design and Characterization," *IEEE Trans. Antennas Propag.*, vol. 68, no. 10, pp. 6964–6972, 2020.

[27] G. Maldonado, A. R. Maldonado, L. I. Balderas, and M. A. Panduro, "Time-Modulated Antenna Arrays for Ultra-Wideband 5G Applications," *Micromachines*, vol. 13, no. 12, 2022.

[28] G. Ni, C. He, and R. Jin, "Harmonic-Based MIMO Transceiver With Time-Modulated Arrays," *IEEE Transactions on Antennas and Propagation*, vol. 71, no. 9, pp. 7553–7565, 2023.

[29] Q. Zhu, S. Yang, R. Yao, and Z. Nie, "Directional Modulation Based on 4-D Antenna Arrays," *IEEE Transactions on Antennas and Propagation*, vol. 62, no. 2, pp. 621–628, 2014.

[30] J. Guo, L. Poli, M. A. Hannan, P. Rocca, S. Yang, and A. Massa, "Time-Modulated Arrays for Physical Layer Secure Communications: Optimization-Based Synthesis and Experimental Assessment," *IEEE Trans. Antennas Propag.*, vol. 66, no. 12, pp. 6939–6949, 2018.

[31] C. He, Q. Chen, A. Cao, J. Chen, and R. Jin, "Application of the Time Modulated Array in Satellite Communications," *IEEE Wireless Communications*, vol. 26, no. 2, pp. 24–30, 2019.

[32] I. Kanbaz, G. O. Arican, Z. Noamadeh, and E. Aksoy, "An Optimization Approach to Synthesis of the Isoflux Pattern for GEO/MEO Satellites using Time Modulated Antenna Arrays," in *Signal Processing and Communications Applications Conference*, 2022, pp. 1–4.

[33] G. G. Lema, A. Bandi, E. Lagunas, B. S. Mysore R, and J. Grotz, "TMA-Based Beamforming for Next Generation Satellite Communication Applications," in *2024 IEEE International Conference on Communications*, 2024, pp. 1919–1925.

[34] L. You and et.al, "Massive mimo transmission for leo satellite communications," *IEEE Journal on Selected Areas in Communications*, vol. 38, no. 8, pp. 1851–1865, 2020.

[35] F. Tang, Q. Wang, C. Zhu, J. Huang, and W. Zhou, "Multicast multigroup beamforming for frame-based leo satellite communications," in *2024 9th International Conference on Computer and Communication Systems (ICCCS)*, 2024, pp. 805–810.

[36] A. Safaai-Jazi, "A new formulation for the design of Chebyshev arrays," *IEEE Trans. Antennas Propag.*, vol. 42, no. 3, pp. 439–443, 1994.

[37] S.-R. Zhang, Y.-X. Zhang, and C.-Y. Cui, "Efficient Multiobjective Optimization of Time-Modulated Array Using a Hybrid Particle Swarm Algorithm With Convex Programming," *IEEE Antennas and Wireless Propagation Letters*, vol. 19, no. 11, pp. 1842–1846, 2020.

[38] S. R. Zhang, Y. X. Zhang, and C.-Y. Cui, "Efficient Multiobjective Optimization of Time-Modulated Array Using a Hybrid Particle Swarm Algorithm With Convex Programming," *IEEE Antennas and Wireless Propagation Letters*, vol. 19, no. 11, pp. 1842–1846, 2020.

[39] G. Ram, D. Mandal, R. Kar, and S. P. Ghosal, "Swarm Optimization Based Side Lobe Reduction in Time Modulated Linear Antenna Arrays," in *International Conference on CICN*, 2014, pp. 1101–1105.

[40] G. G. Lema, G. T. Tesfamariam, and M. I. Mohammed, "A Novel Elliptical-Cylindrical Antenna Array for Radar Applications," *IEEE Trans. Antennas Propag.*, vol. 64, no. 5, pp. 1681–1688, 2016.

[41] S. Cakaj, "The parameters comparison of the 'Starlink' LEO satellites constellation for different orbital shells," *Frontiers in Communications and Networks*, vol. 2, no. 643095, 2021.

[42] O. Abbasi and G. Kaddoum, "Channel aging-aware lstm-based channel prediction for satellite communications," *IEEE Networking Letters*, vol. 6, no. 3, pp. 183–187, 2024.

[43] C. Li, O. El-Aassar, A. Kumar, M. Boenke, and G. M. Rebeiz, "LNA Design with CMOS SOI Process-l.4dB NF K/Ka band LNA," in *IEEE International Microwave Symposium - IMS*, 2018, pp. 1484–1486.

[44] C. Wilson and B. Floyd, "20–30 GHz mixer-first receiver in 45-nm SOI CMOS," in *2016 IEEE Radio Frequency Integrated Circuits Symposium (RFIC)*, 2016, pp. 344–347.

[45] M. Baert and W. Dehaene, "20.1 A 5GS/s 7.2 ENOB Time-Interleaved VCO-Based ADC Achieving 30.5fJ/conv-step," in *2019 IEEE International Solid-State Circuits Conference - (ISSCC)*, 2019, pp. 328–330.

[46] U. Kodak and G. M. Rebeiz, "Bi-directional flip-chip 28 GHz phased-array core-chip in 45nm CMOS SOI for high-efficiency high-linearity 5G systems," in *2017 IEEE Radio Frequency Integrated Circuits Symposium (RFIC)*, 2017, pp. 61–64.

[47] B. Degnan, B. Marr, and J. Hasler, "Assessing Trends in Performance per Watt for Signal Processing Applications," *IEEE Transactions on Very Large Scale Integration Systems*, vol. 24, no. 1, pp. 58–66, 2016.

[48] P. Saha, "A Quantitative Analysis of the Power Advantage of Hybrid Beamforming for Multibeam Phased Array Receivers," *Microw. J*, 2021.

[49] M. N. Dazhi, H. Al-Hraishawi, M. R. B. Shankar, S. Chatzinotas, and B. Ottersten, "Energy-Efficient Service-Aware Multi-Connectivity Scheduler for Uplink Multi-Layer Non-Terrestrial Networks," *IEEE trans. green commun. netw.*, vol. 7, no. 3, 2023.

Gebrehiwet Gebrekrstos Lema (Student Member, IEEE) received the B.Sc in Electronics and Communication Engineering from Mekelle Institute of Technology in 2010 and M.Sc in Communication Engineering from EiT-M in 2015. He worked as a researcher in Germany and as a lecturer and quality assurance head of EiT-M, Mekelle University. Presently, he is pursuing a Ph.D. from the University of Luxembourg, Luxembourg. His research interest focuses on emerging onboard processing for next-generation satellite communications, beamforming designs, optimization techniques, antenna designs, machine learning, and free-space optical communications.

Eva Lagunas (Senior Member, IEEE) received the M.Sc. and Ph.D. degrees in telecommunications engineering from the Polytechnic University of Catalonia (UPC), Barcelona, Spain, in 2010 and 2014, respectively. She has held positions with Centre Tecnologic de Telecommunications de Catalunya (CTTC), UPC, the University of Pisa, Italy; and the Center for Advanced Communications (CAC), Villanova University, PA, USA. In 2014, she joined the Interdisciplinary Centre for Security, Reliability, and Trust (SnT), at the University of Luxembourg, where she currently holds a research scientist position. Her research interests include terrestrial and satellite system optimization, spectrum sharing, resource management, and machine learning.

M. R. Bhavani Shankar (Senior Member, IEEE) received the master's and Ph.D. degrees in electrical communication engineering from the Indian Institute of Science, Bangalore, in 2000 and 2007, respectively. He was a Post-Doctoral Researcher with the ACCESS Linnaeus Centre, Signal Processing Laboratory, Royal Institute of Technology (KTH), Sweden, from 2007 to September 2009. He joined SnT in October 2009 as a Research Associate and is currently an Assistant Professor with the Signal Processing Applications in Radar and Communications (SPARC) Group. He was a Visiting Student with the Communication Theory Group, ETH Zurich, headed by Prof. Helmut Bölcskei, in 2004. His research interests include design and optimization of MIMO communication systems, automotive radar and array processing, polynomial signal processing, satellite communication systems, resource allocation, game theory, and fast algorithms for structured matrices. He was a co-recipient of the 2014 Distinguished Contributions to Satellite Communications Award from the Satellite and Space Communications Technical Committee, IEEE Communications Society. He is currently on the Executive Committee of the IEEE Benelux Joint Chapter on Communications and Vehicular Technology and serves as the Handling Editor for Signal Processing (Elsevier).

Joel Grotz (Senior Member, IEEE) received the joint degree in electrical engineering from the University of Karlsruhe and the Grenoble Institute of Technology in 1999 and the joint Ph.D. degree in telecommunications from the University of Luxembourg and KTH, Stockholm, in 2008. He was with SES, Betzdorf, Luxembourg, on the development of satellite broadband communication system design for GEO and MEO high-throughput satellite systems on different ground segment and space segment topics and system optimization aspects. He was with the Technical Laboratories, ST Engineering iDirect (former Newtec Cy with Sint-Niklaas, Belgium) on topics of system design and signal processing in satellite modems. He is currently the Senior Manager of SES on the development of a dynamic resource management system for novel flexible satellite systems, including SES-17 and O3b mPOWER and future satellite systems under planning.